Materials Science and Engineering R 46 (2004) 1–49

R Reports: A Review Journal

www.elsevier.com/locate/mser

Available online at www.sciencedirect.com

SCIENCE DIRECT®

Multiphase solidification in multicomponent alloys

U. Hecht[a,*], L. Gránásy[b], T. Pusztai[b], B. Böttger[a], M. Apel[a], V. Witusiewicz[a], L. Ratke[c], J. De Wilde[d], L. Froyen[d], D. Camel[e], B. Drevet[e], G. Faivre[f], S.G. Fries[a], B. Legendre[g], S. Rex[a]

[a]*ACCESS e.V, Aachen, Germany*
[b]*Research Institute for Solid State Physics and Optics of the Hungarian Academy of Sciences, Budapest, Hungary*
[c]*Institute of Space Simulation DLR Köln, Germany*
[d]*Departement MTM, Katholieke Universiteit Leuven, Faculteit toegepaste wetenschappen, Leuven, Belgium*
[e]*CEA-Grenoble, Grenoble, France*
[f]*Groupe de Physique des Solides (GPS), Université Paris 6, Paris, France*
[g]*Laboratoire de Chimie Physique Minérale et Bioinorganique, EA 401, Faculté de Pharmacie, Châtenay-Malabry, France*

Available online 8 September 2004

Abstract

Multiphase solidification in multicomponent alloys is pertinent to many commercial materials and industrial processes, while also raising challenging questions from a fundamental point of view. Within the past few years, research activities dedicated to multiphase solidification of ternary and multicomponent alloys experienced considerable amplification. This paper gives an overview of our present understanding in this field and the experimental techniques and theoretical methods research relies on. We start with an introduction to thermodynamic databases and computations and emphasize the importance of thermophysical property data. Then, we address pattern formation during coupled growth in ternary alloys and cover microstructure evolution during successive steps of phase formation in solidifying multicomponent alloys. Subsequently, we review advances made in phase field modeling of multiphase solidification in binary and multicomponent alloys, including various approaches to crystal nucleation and growth. Concluding, we address open questions and outline future prospects on the basis of a close interaction among scientists investigating the thermodynamic, thermophysical and microstructural properties of these alloys.

Keywords: Solidification; Multicomponent alloys; Multiphase microstructures; Thermodynamics; Phase field simulation; Nucleation

1. Introduction

Many commercial materials are multicomponent, multiphase alloys, whose properties are determined by the microstructure that develops during solidification and subsequent processing stages. One of the essential challenges to materials science is to understand how multiphase microstructures form and how they can be controlled via deliberate selection of alloy composition and processing parameters. Design of materials optimized for specific applications presumes a detailed understanding of microstructure formation and reliable databases for all the relevant properties. Such a knowledge-based approach will improve the efficiency of industrial R&D by reducing the cost and time of product development. Its realization, however, needs a concerted effort of the materials science community.

* Corresponding author. Tel.: +49 241 8098014; fax: +49 241 38578.
E-mail address: ulrike.hecht@access.rwth-aachen.de (U. Hecht).

0927-796X/$ – see front matter
doi:10.1016/j.mser.2004.07.002

In the case of binary alloys, a manifold of dedicated models and comprehensive simulation tools have been developed for predicting microstructure formation. This holds for solidification and solid-state transformations of binary single-phase and multiphase materials. Some of the thermodynamic properties required for modeling can be read off the phase diagram of the alloy under consideration and many of the thermophysical properties are also available from literature.

For multicomponent alloys with three or more components, the process of microstructure formation during solidification is less understood, especially for cases where multiphase reactions occur along the solidification path of the alloy. Such cases are common in industrial practice, therefore, R&D efforts are directed towards (i) avoiding microsegregation associated with the formation of detrimental minority phases and (ii) controlling the amount, the morphology, and distribution of the beneficial minority phases.

Well-known detrimental phases are brittle intermetallic compounds, i.e. G-phases like $(Ni, Co)_{16}(Ti, Cr)_6Si_7$ in Ni–Co–Cr–Si superalloys [1] or $Ni_{16}Mg_6Si_7$ in Cu–Ni–Si alloys and sigma-phases in Cr- and Mo-rich Ni-base [2] or Co-base alloys [3]. In aluminum alloys, a series of Fe-, Mn- and Si-rich intermetallic phases [4] can cause severe problems during thermomechanical treatment or during service of as cast materials. Beneficial minority phases, like carbides in different grades of steel, Ni-aluminides in Al-bronzes for wear applications, 211-particles for flux pinning in YBaCuO-superconductors, silicon particles in aluminum alloys for automotive pistons, etc. do not need to be mentioned here in more detail.

Fig. 1 shows three representative examples of multiphase microstructure formed during solidification of commercial materials.

Other multiphase materials, often termed in situ composites, are currently being developed. Such materials contain high amounts of secondary or tertiary phases that may be distributed as discrete particles, lamellae or fibers within the matrix phase. Typical examples are intermetallics for structural application at high temperatures, such as Laves-phase strengthened NiAl-intermetallics from NiAl–7.5Cr–2.5Ta alloys [5]. Directionally solidified eutectic ceramics, e.g. $Al_2O_3/ZrO_2(Y_2O_3)$ are expected to achieve better high temperature creep resistance [6] than single phase ceramics. Steep refractive index profiles associated with the aligned microstructure of ZrO_2–CaO [7] and CaF_2–MgO [8] eutectics make them promising candidates for planar and fiber optical waveguiding.

Multiphase solidification of multicomponent materials attracts pronounced academic interest as well. Outstanding problems are the morphological stability in such systems and the nature and dynamic behavior of the multiphase patterns forming in coupled growth. This is an especially challenging field, as the high number of degrees of freedom and the multiplicity of phases lead to phenomena specific to only such complex systems. In this regard, ternary alloys serve as example. Growth of two solid phases from the liquid, e.g. in eutectic reaction, is no longer nonvariant as in

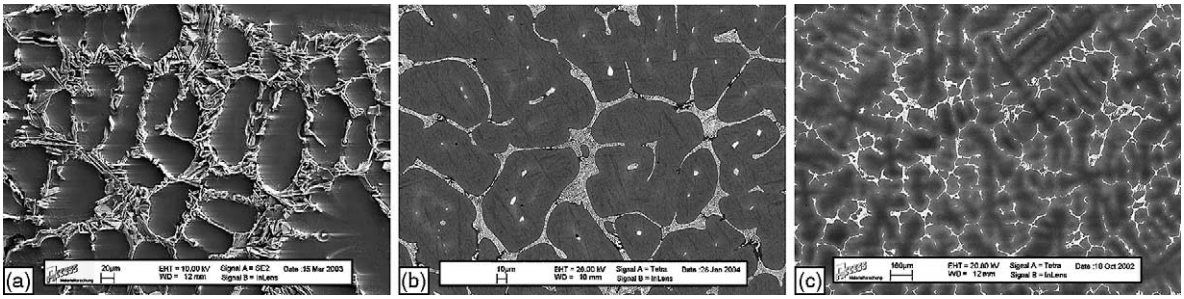

Fig. 1. Multiphase microstructures formed in the terminal stages of solidification in (a) Al–Si 7–Mg 0.6—as cast, (b) Fe–C 0.9–Cr 4–Mo 5–W 6.5—thixo cast, (c) Cu–Sn 12–Ni 2—as cast.

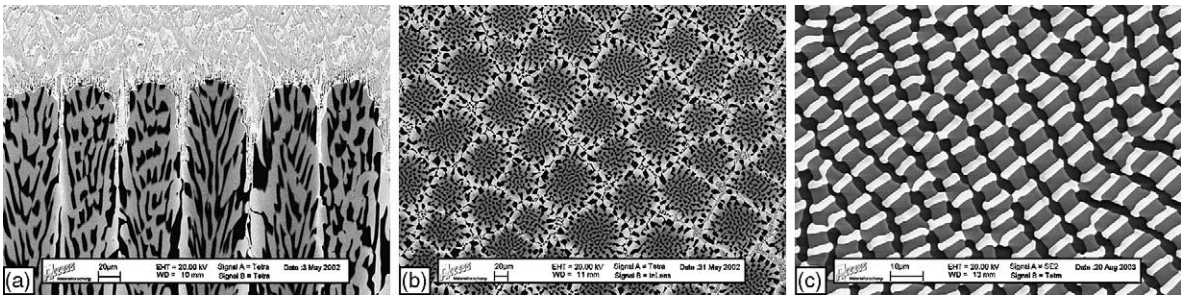

Fig. 2. Multiphase patterns in ternary Al–Cu–Ag alloys after unidirectional solidification: eutectic cells in longitudinal (a) and cross section (b) of Al–Cu 13.66 at.%–Ag 10.27 at.% and a three-phase eutectic pattern (c) in cross section of Al–Cu 13.6 at.%–Ag 16.4 at.%.

binary alloys but is univariant. Accordingly, the two-phase solid/liquid interface can exhibit morphological transitions to cellular or dendrite-like patterns. Nonvariant growth in a ternary alloy involves three solid phases growing simultaneously from the liquid, thus the respective patterns are more complex then in binary (nonvariant) eutectics. Fig. 2 shows multiphase patterns formed during unidirectional solidification of ternary eutectic alloys.

The industrial and fundamental aspects of multiphase microstructure evolution in multicomponent alloys can only be addressed with the hope for success, if a close interaction is maintained among scientists investigating the thermodynamic, thermophysical, and microstructural properties of these alloys. In this paper, we review recent advances experiment and theory made in these areas.

This paper is based on discussions within the topical team ''Solidification in Multicomponent Multiphase Systems''. The team was organized and funded by the European Space Agency ESA with the intention to stimulate the interaction between research groups from university and industry and to establish the scientific background for future experiments in microgravity.

2. Thermodynamic databases and computational thermodynamics

For binary alloy systems both constructing and reading phase diagrams is quite easy. But with increasing number of alloying elements the amount of data required to construct a phase diagram increases significantly and also reading is no longer straightforward. The way through to resolve such problems is using computational thermodynamics, that encompasses the creation of thermodynamic databases based on the CALPHAD method developed by Kaufman [9] and recently reviewed by Saunders [10] and their use in calculation of phase equilibria with appropriate software.

Today a unary database exists and was published in 1991 by Dinsdale [11]. This database describes the Gibbs energy of 78 elements in different stable and metastable states as functions of temperature and pressure. It has become the standard reference used with the CALPHAD method. The unary descriptions were adopted internationally. A similar work is being done for binary systems for which the Gibbs energy of all phases in each system are modeled (SGTE [12]). At present about 400 binary systems have assessed thermodynamic descriptions out of the 3080 possible combinations of the elements from the unary database. For ternary or quaternary systems no critically reviewed and internationally adopted assessments are available, but quite some descriptions, often more then one for a given system, are published in literature. The availability of comprehensive multicomponent databases is much biased by industrial demand. Today such databases are available for Fe-base

alloys, for Ni-base superalloys, for Al-based light alloys, for Ti and TiAl based alloys, for solders and few others like slag and geochemical systems.

In what follows we give a short introduction on the methodology of database construction and describe experimental and computational methods that yield the thermodynamic data needed for database construction. Finally we discuss the use of thermodynamic databases in thermodynamic calculations and their contribution to our understanding of microstructure formation.

2.1. Thermodynamic databases and thermodynamic data

A thermodynamic database gives a parametric description of the Gibbs free energy for all phases of the considered alloy system as function of temperature, composition and pressure. The free parameters are adjusted such that all available discrete data related to the Gibbs free energy and its derivatives are recovered at best. The parametric description is based on Gibbs free energy models that account for the specific crystal structures of the individual phases, e.g. substitutional solution phases, stoichiometric compounds and ordered phases. For the latter the so called sublattice model was developed by Hillert [13] and extended by Sundman [14]. It can be also applied to a variety of solution phases.

For a ternary substitutional solution phase ϕ, the molar Gibbs energy is expressed as [10]:

$$G_{\mathrm{m}}^{\phi} = G_{\mathrm{m}}^{\phi,\mathrm{ref}} + G_{\mathrm{m}}^{\phi,\mathrm{id}} + G_{\mathrm{m}}^{\phi,\mathrm{xs}} \tag{1}$$

The terms represent reference, ideal mixing and excess contributions as follows.

The reference term corresponds to a simple mechanical mixture of the Gibbs energy of the constituent components:

$$G_{\mathrm{m}}^{\phi,\mathrm{ref}} = \sum_{i=1}^{n} x_i \, G_i^{\circ}(T) \tag{2}$$

The temperature dependence of $G_i^{\circ}(T)$ is formulated as a power series of T:

$$G_i^{\circ}(T) = a + bT + cT\ln(T) + \sum d_n T^n \tag{3}$$

The ideal mixing term in Eq. (1) corresponds to the entropy of mixing for an ideal solution,

$$G_{\mathrm{m}}^{\phi,\mathrm{id}} = RT \sum_{i=1}^{n} x_i \ln(x_i) \tag{4}$$

and the excess term to deviations form ideal mixing that are due to specific interactions between the components.

$$G_{\mathrm{m}}^{\phi,\mathrm{id}} = \sum_{i=1}^{n-1} \sum_{j=i+1}^{n} x_i x_j \, L_{i:j}^{\phi} \quad \text{with} \quad L_{i:j}^{\phi} = \sum_{\nu=0}^{k} (x_i - x_j)^{\nu} \, L_{i:j}^{\nu,\phi} \tag{5}$$

Here, x_i is the molar fraction of component i, L_{ij}^{ν} are pairwise interaction parameters that can be temperature dependent according to an expression similar to (3):

$$L_{i:j}^{\nu,\phi} = a_{i:j}^{\nu,\phi} + b_{i:j}^{\nu,\phi} T + c_{i:j}^{\nu,\phi} \ln T + \sum d_{i:j}^{\nu,\phi} T^n \tag{6}$$

As can be seen from Eq. (5) three pairwise contributions to the excess term are needed for a ternary phase. The respective pairwise interaction parameters can be taken from the assessed binary databases or be subject to fitting. If experimental information relative to ternary interaction is

available, then an extra term is added to Eq. (5) as to account for the ternary interaction, giving [15]:

$$G_{\mathrm{m}}^{\phi,\mathrm{xs}} = \sum_{i=1}^{n-1}\sum_{j=i+1}^{n} x_i x_j L_{i:j}^{\phi} + \sum_{i=1}^{n-2}\sum_{j=i+1}^{n-1}\sum_{k=j+1}^{n} x_i x_j x_k L_{i:j:k}^{\phi} \tag{7}$$

As illustrated here for the case of a ternary substitutional phase, several free parameters are entering the description, their number grows with the number of phases that need to be modeled for a given alloy system. Some of the parameters can be taken over from the assessed databases of the lower order subsystems, as the strategy of database construction is necessarily hierarchical. Nonetheless, reliable discrete data are needed for fitting the remaining parameters. Most of such data originate form experimental measurements: A series of dedicated experimental techniques are available and have been described in a comprehensive way by Kubaschewski [16].

The following example from Witusiewicz et al. [17] is meant to show how much experimental effort is indeed underlying the development of a thermodynamic database: The experiments were dedicated to measuring the partial and the integral enthalpies of mixing of ternary liquid Ag–Al–Cu alloys at a temperature of 1252 ± 5 K by isoperibolic calorimetry.

Fig. 3 shows the compositions of liquid ternary Ag–Al–Cu alloys investigated as to supplement already available data for Al-rich liquid alloys, published by Flandorfer and Hayer [18]. For the sake of clearness we reproduce here the results for the integral enthalpy of mixing only.

Fig. 4 shows the experimentally measured values of the integral enthalpy of mixing as function of the aluminum content (solid symbols), data from [18] (hollow symbols) and fits of the discrete data based on the Redlich–Kister–Muggianu polynomial equation [15] for the excess contributions to mixing:

$$\Delta H_{\mathrm{m}}^{\phi,\mathrm{xs}} = \sum_{i=1}^{n-1}\sum_{j=n+1}^{n} x_i x_j a_{i:j}^{v,\phi} + \sum_{i=1}^{n-2}\sum_{j=i+1}^{n-1}\sum_{k=j+1}^{n} x_i x_j x_k a_{i:j:k}^{\phi} \tag{8}$$

All parameters needed for thermodynamic modeling of the liquid phase in the entire Al–Cu–Ag system are summarized in Table 1.

Fig. 5 finally shows the isolines of the integral enthalpy of mixing of liquid Ag–Al–Cu alloys at 1252 ± 5 K on a Gibbs triangle calculated according to Eq. (8) with the parameters listed in Table 1.

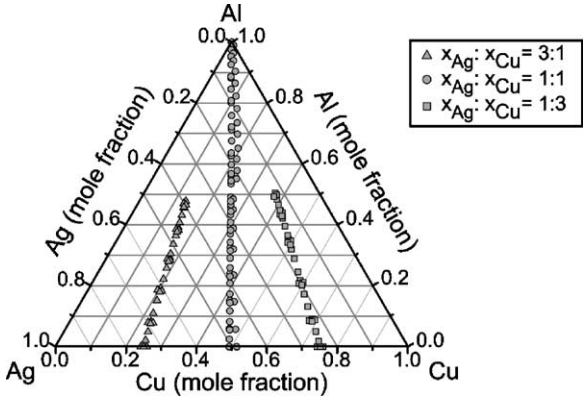

Fig. 3. Composition of liquid ternary alloys prepared during measurement of the partial and integral enthalpy of mixing by isoperibolic calorimetry. The compositions are obtained successively by dissolving the appropriate amount of pure components in the liquid mixture stemming from the previous dissolution step.

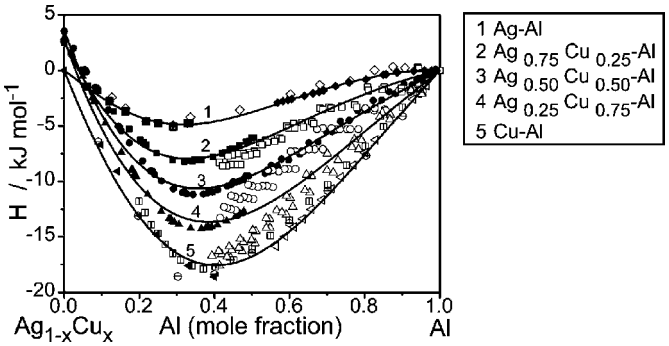

Fig. 4. Integral enthalpy of mixing of liquid Ag–Al–Cu alloys at 1252 ± 5 K as function of the Al-content. The symbols present experimental data by [17] (solid) and [18] (hollow). The solid curves represent fits according to Eq. (8) with the parameters summarized in Table 1.

Table 1
Parameters of the liquid Ag–Al–Cu at 1252 ± K referred to liquid constituents

Parameter symbol	Binary interaction parameters (J mol^{-1})				
	$v = 0$	$v = 1$	$v = 2$	$v = 3$	$v = 4$
$a^{v,\phi}_{\mathrm{Ag:Al}}$	−14187	−20340	−4834	5555	8726
$a^{v,\phi}_{\mathrm{Ag:Cu}}$	14462	−934			
$a^{v,\phi}_{\mathrm{Al:Cu}}$	−67094	32148	5915	−8175	
	Ternary interaction parameters (J mol^{-1})				
	$\alpha^{\phi}_{\mathrm{Ag}}$	$\alpha^{\phi}_{\mathrm{Al}}$	$\alpha^{\phi}_{\mathrm{Cu}}$		
a^{ϕ} see Eq. (8)	−131340	−38140	−65997		

For a complete database of the ternary system Ag–Al–Cu thermodynamic modeling of all solid phases is needed as well. For each of the phases, not only the chemical composition (solubility range), crystal structure and lattice decoration but also thermodynamic properties are needed. The latter include both, enthalpies and entropies that characterize the Gibbs free energy of a phase as function of

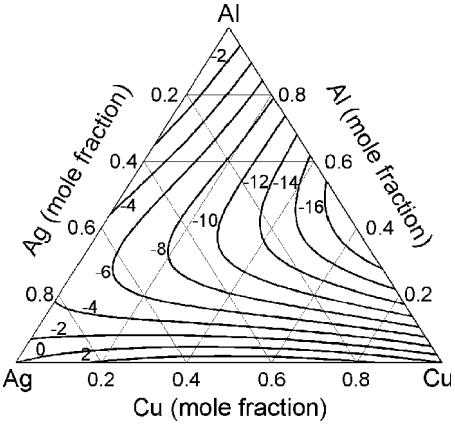

Fig. 5. Integral enthalpy of mixing of liquid Ag–Al–Cu alloys at 1252 ± 5 K presented as iso-enthalpy curves on the Gibbs triangle of the Ag–Al–Cu system.

temperature, pressure and composition. Isoperibolic calorimetry, differential scanning calorimetry and activity measurements by the EMF or Knudsen cell technique are usually applied for individual phases. For the detection of phase transitions DTA, dilatometry and in situ XRD studies are best suited. With regard to such task, the advantage of the CALPHAD method becomes fully evident, as assessed data from different sources may be used together, including data form lower order subsystems.

Since computational power and the accuracy of computational methods significantly increased, first-principle calculations of thermodynamic properties start becoming a valuable source of thermodynamic data. In a recent overview Asta et al. [19] reported on applications of first principle calculations to the study of bulk and interfacial thermodynamic properties. Among others Fries and Sundman [20] showed a way to integrate first-principle calculations into the compound energy formalism commonly used within the CALPHAD method for modeling the Gibbs energy of intermetallic phases with a wide range of solubility. The method was applied to modeling the Sigma-Phase in the binary system W–Re. Gosh et al. [21] demonstrated a hybride approach to integrate the results of first-principle calculations with the CALPHAD formalism to obtain thermodynamic data for the Hf–Nb system. For dilute ternary alloys only few first principle studies are available [22] and remain a challenge for concentrated ternary alloys. None the less, the power of first principle calculations and atomistic simulations for both bulk and interfacial thermodynamic properties opens up a promising perspective.

2.2. Applications of computational thermodynamics

Once available, thermodynamic databases combined with numerical codes [23–27] able to calculate total Gibbs energy minima (thermodynamic equilibria) at any composition, temperature and pressure are highly effective to handle complex phase equilibria. Very instructive reviews on applications of computational thermodynamics are published by Kattner et al. [28,29] and Ågren et al. [30]. Looking at the manifold applications that indeed are daily practice within many industrial R&D projects, it becomes evident that thermodynamic computations are the most advanced tool for tackling solidification of multicomponent, multiphase materials. Most frequently equilibrium or Scheil calculations of the solidification path are being performed to compute the type and amount of phases present in a given alloy as function of temperature.

In the following we present an application that aims at calculating the formation of delta-ferrite as function of the carbon content in high carbon steels being used for production of hot rolling cylinders by centrifugal casting. The example is given by courtesy of Gonterman and Peipers, Germany. A typical composition of the steel, given in wt.%, is Fe–C 0.45%–Mo 1%–Si 0.5%–V 0.5%–Cr 5%–Ni 0.5%–Mn 0.7%. The high carbon content, together with significant amounts of carbide forming elements is meant to increase the fraction of carbides and hence the wear resistance. But with increasing amount of carbide forming elements, the peritectic reaction liquid + δ-ferrite → austenite is shifted to higher carbon contents. In the isopleth of Fig. 6 the influence of chromium on the peritectic reaction in ternary Fe–C–Cr alloys is depicted. In order to avoid the formation of δ-ferrite during solidification, the carbon content of the multicomponent alloy must be adjusted. Thermodynamic equilibrium calculations using an appropriate database can easily handle this task. Fig. 7 summarizes the results of such a calculation performed with Thermo-Calc [23] and the database TC-Fe. The plots show the mole fraction of δ-ferrite as function of temperature, first increasing with decreasing temperature as primary phase in equilibrium with the liquid, then decreasing during the peritectic reaction. Similar plots for the evolution of the mole fraction of all other phases in the alloy can be equally obtained, if needed.

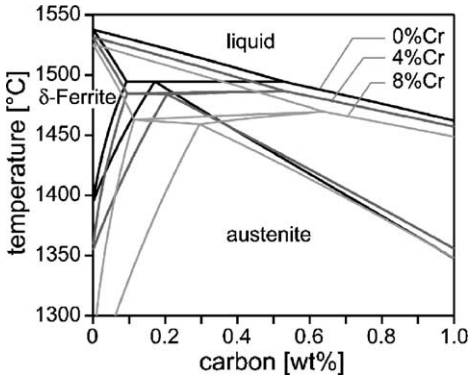

Fig. 6. With increasing Cr-content in ternary Fe–C–Cr alloys the δ-ferrite field extends to higher carbon content than in the binary Fe–C system.

The following application aims at computing the thermodynamic equilibrium data that are necessary for the characterization of univariant eutectic growth in a ternary alloy system. The alloy system under consideration is Al–Cu–Ag and the univariant eutectic reaction of interest is liquid → $\alpha(Al) + Al_2Cu$. The univariant eutectic groove associated to this reaction is marked as no.1 within the projection of the liquidus surface of Al–Cu–Ag presented in Fig. 8. Table 2 contains the composition of the phases in equilibrium along this groove as computed with Thermo-Calc [23] and the database developed by Witusiewicz et al. [31]. The compositions correspond to the corners of the tie triangle at the indicated temperature. For $T = 505\ ^{\circ}C$ the isothermal section through the system Al–Cu–Ag is shown in Fig. 9 and the relevant tie triangle is marked as no. 1, as to distinguish it more easily from other tie triangles.

For unidirectional solidification of univariant eutectic alloys in steady state, tie triangles contain all the information about the thermodynamic equilibrium at the solid/liquid interface in the limit of zero growth velocity. Such tie triangles are depicted in Fig. 10. They uniquely determine the equilibrium temperature, the composition of the phases in equilibrium, and the mole fraction of the solid phases inside the eutectic. This allows for calculation of the phase-weighted integral composition of the solid. For alloys with exactly on-groove compositons the calculated values are given in Table 3. In Fig. 11 the integral solid compositions and the compositions of the liquid in equilibrium with the two-phase solid are plotted as function of the temperature for the entire univariant

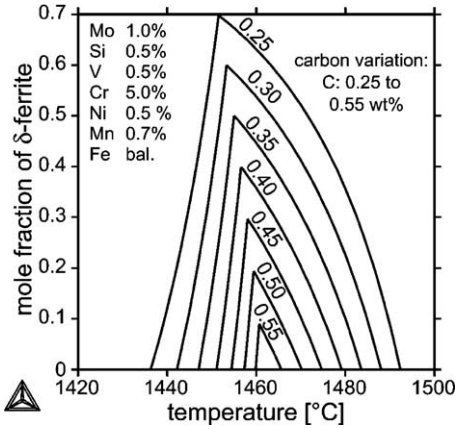

Fig. 7. Evolution of the mole fraction of δ-ferrite with temperature for different carbon contents of the multicomponent alloy.

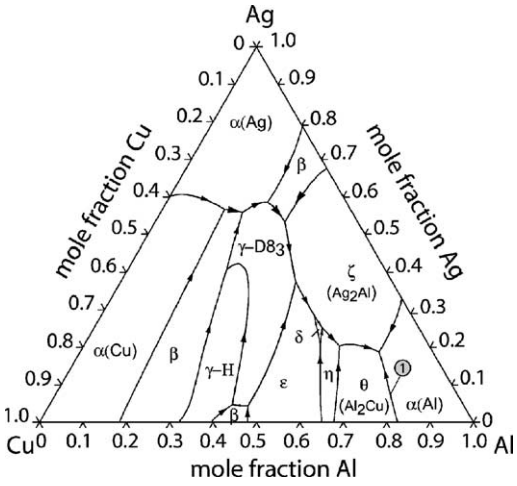

Fig. 8. Univariant and nonvariant reactions on the liquidus surface of the Al–Cu–Ag system.

Table 2
Phases in equilibrium for the univariant eutectic reaction: liquid → α(Al) + Al_2Cu

Temperature (°C)	Calculated composition of phases in equilibrium (at.%)					
	α(Al)		Al_2Cu		Liquid	
	Ag	Cu	Ag	Cu	Ag	Cu
502.2	15.910	5.063	0.0427	32.291	18.573	12.413
505.0	11.160	4.625	0.0415	32.259	16.700	12.754
510.0	7.451	3.846	0.0389	32.204	14.238	13.435
515.0	5.579	3.408	0.0358	32.150	11.879	14.068
520.0	4.227	3.213	0.0322	32.098	9.659	14.652
525.0	3.256	3.018	0.0281	32.047	7.613	15.334
530.0	2.390	2.969	0.0235	31.998	5.671	15.967
535.0	1.627	2.775	0.0184	31.950	3.902	16.356
540.0	0.899	2.677	0.0128	31.903	2.202	16.940

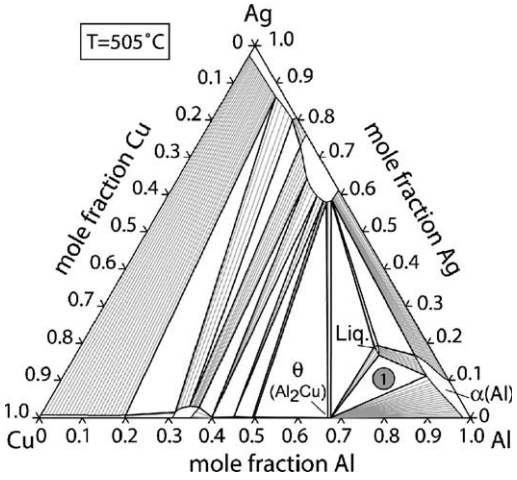

Fig. 9. Isothermal cut through the phase diagram of the ternary alloy system Al–Cu–Ag at T = 505 °C.

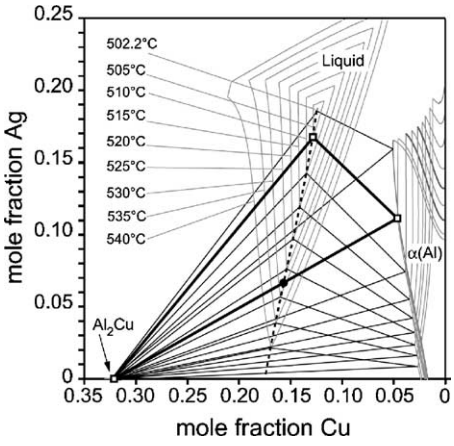

Fig. 10. Tie triangles calculated for the univariant eutectic reaction liquid → α(Al) + Al_2Cu. The bold tie triangle shows the composition of the phases in equilibrium at the solid/liquid interface (hollow squares) for the on-groove alloy marked with a solid circle. From the lever rule applied to the tie line between α(Al) and Al_2Cu the mole fractions of the two phases can be determined.

Table 3
Mole fractions of the solid phases and integral composition of the solid for steady state growth of on-groove alloys in the limit of zero growth velocity (thermodynamic equilibrium)

Temperature (°C)	Mole fraction of solid phases		Integral composition of the solid	
	α(Al)	Al_2Cu	Ag (at.%)	Cu (at.%)
502.2	0.648	0.351	10.331	14.633
505.0	0.600	0.400	6.710	15.681
510.0	0.561	0.439	4.197	16.292
515.0	0.535	0.465	3.000	16.784
520.0	0.519	0.481	2.211	17.115
525.0	0.509	0.491	1.677	17.262
530.0	0.501	0.499	1.215	17.469
535.0	0.491	0.509	0.818	17.616
540.0	0.485	0.515	0.455	17.725

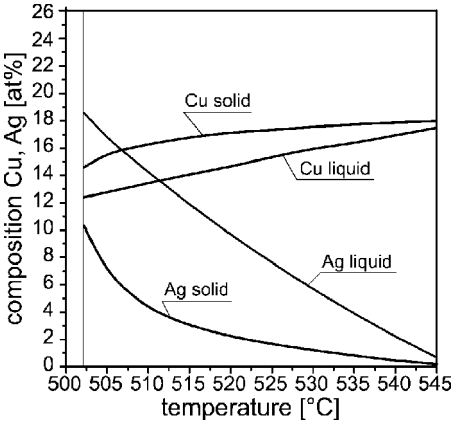

Fig. 11. Partition of Ag and Cu between the eutectic solid (consisting of α(Al) and Al_2Cu) and the liquid at solid/liquid interfaces of univariant eutectic alloys with integral on-groove compositions. Below 502.2 °C, corresponding to the temperature of the nonvariant eutectic, no univariant equilibrium persists.

groove. Based on these data one can calculate the constitutional supercooling criterion limit for the planar univariant eutectic growth, as will be detailed in Section 4.

While thermodynamic calculations as such are quite versatile and efficient for providing global features of an equilibrium microstructure, they convey however no information on the local arrangement of the phases in the microstructure, e.g. the size distribution and morphology of the individual phases, the neighborhood relationships of the multiphase pattern etc. These features are dependent on the growth kinetics, e.g. on the dissipation of heat and solute generated at the solid/liquid interface(s) under the conditions imposed by the solidification process. The solid/liquid interface(s) are moving free boundaries that adjust their local curvature in order to enhance heat and mass dissipation under the constraints imposed by interfacial energy. Coupling the thermodynamic calculations to other microstructure evolution models is the necessary step, when aiming to understand and eventually predict microstructures in multicomponent alloys. The kinetic software DICTRA [32] is the first to truly integrate thermodynamic calculations with diffusion controlled transformation kinetics for 1D systems. Diffusion is treated based on the chemical potential gradients as driving force, thus allowing to include diffusion against composition gradients (up-hill diffusion). The diffusivities are expressed via mobilities and Darken's thermodynamic factor according to the formalism developed by Ågren [33] and Andersson and Ågren [34]. A variety of DICTRA simulations for steels, recently published by Inden [35], demonstrates the capability and the limitations of the software.

Kraft and Chang [36] succeeded to give a comprehensive overview of microsegregation models in multicomponent alloys. Progress in this field has been achieved by coupling the models to thermodynamic databases. In Section 4.3 we briefly discuss the latest developments in this area. Since recent, the coupling between thermodynamic calculations and phase field simulations for modeling microstructure evolution in multicomponent, multiphase alloys advanced. In Section 5 some of the latest achievements are presented.

3. Thermophysical properties

This section addresses two of the most important thermophysical properties that impact on microstructure evolution during solidification, diffusion coefficients and interfacial energies.

In the absence of convection, diffusion is the only transport mechanism for the dissipation of both heat and solute from the moving interface into the system. Many experiments have been done to measure the intrinsic mobility, also called self-diffusivity or tracer diffusivity, which is a measure of how a component diffuses in the absence of chemical gradients. One can also measure how fast a component diffuses due to its own chemical gradient, thus assessing effective binary diffusion coefficients. In a multicomponent solution phase consisting of "n" components the diffusion of each component is however affected by the chemical gradients of all other components. This makes diffusion in multicomponent, even in simple, substitutional phases quite more complicated. In Section 3.1 a brief overview of methods that can be applied for the determination of the diffusivity matrix are given.

The free energy of a solid/liquid interface is responsible for preserving stability against all perturbations of the interface, while the anisotropy of the surface free energy, resulting from the crystalline anisotropy of the solid, effectively controls the details of morphological destabilization and the shape of the emerging morphological patterns. The important role of even week anisotropy has been recognized for single-phase growth, e.g. for the stability of cellular arrays Kopczyński et al. [37] and the operating point of dendrites Langer [38], Ben Jacob [39]. Determining the solid/liquid

interfacial free energy and ansiotropy is a delicate task even for single component systems. For binary or multicomponent alloys the composition profiles across an interface and interfacial adsorption at the interface renders the problem more difficult. In Section 3.2 we only guide the reader to some methods that have successfully been applied to binary alloys and point out the lack of data for ternary and multicomponent alloys.

3.1. Multicomponent diffusion

In the linear theory developed by Onsager [40] the fluxes J_i of the components $i = 1, \ldots, n$ are expressed as linear functions of the driving forces. In a very general form, the driving forces may be expressed as potential gradients $\bigtriangledown\phi_j$, where the potentials ϕ_j are functions of composition, i.e. chemical potentials.

$$J_i = -\sum_{j=1}^{n} L_{ij} \nabla\phi_j \tag{9}$$

The phenomenological parameters L_{ij} relate the flux of component i to the potential gradients $\bigtriangledown\phi_j$ of all other components. The parameters L_{ij} are the elements of an $n \times n$ matrix and the potential gradients constitute n interdependent driving forces for diffusion, typically chemical potential gradients. This expression holds for isothermal diffusion, i.e. when cross effects with thermal gradients or other field gradients may be neglected. Eq. (9) can be reduced to a set of $(n - 1)$ independent equations with $(n - 1)^2$ coefficients, based on the Gibbs–Duhem law and more, can be transformed to different frames, depending on the frame of reference within which the fluxes are expressed. The procedures of reduction and frame transformation are described in Kirkaldy's monograph on diffusion in the condensed state [41] and extended by Ågren [33] and Anderson and Ågren [34]. For practical situations, when diffusion is treated in the volume-fixed frame of reference and the driving forces are expressed via concentration gradients, rather than chemical potential gradients, the fluxes are [34]:

$$J_i = -\sum_{j=1}^{n-1} D_{ij}^{n} \nabla c_j \tag{10}$$

The coefficients D_{ij}^{n}, so-called chemical diffusivities, constitute an $(n - 1) \times (n - 1)$ diffusivity matrix. The superscript n denotes the choice of the solvent, which represents the dependent component. Because the chemical diffusivities relate to concentration gradients instead of chemical potential gradients, they include thermodynamic factors in addition to diffusion kinetic terms.

As Fick's second law applies,

$$\frac{\partial c_i}{\partial t} = -\mathrm{div}(J_i) \tag{11}$$

the coefficients of the diffusivity matrix can be determined from measured concentration profiles, typically from diffusion couples designed to achieve 1D fluxes. Two software packages are available to assess the chemical diffusivity matrix form one-dimensional multicomponent diffusion data obtained from diffusion couples: Profiler is based on the square root diffusivity method, developed by Brockman and Morral [42] and provides a practical solution to 1D multicomponent diffusion, whenever the chemical diffusivities are constant. DICTRA is based on the diffusion mobility formalism developed by Ågren [33] and Anderson and Ågren [34] and treats concentration dependent chemical diffusivities, by expressing the activation energy for diffusion in a Redlich–Kister poly-

nomial form. DICTRA takes advantage of the fact that the thermodynamic factors can be calculated directly from thermodynamic databases, when available. Both methods have been extensively used to assess solid state diffusion in multicomponent alloys. Here we give just two references: Cohen and Glicksman [43] investigated diffusion path shapes in ternary Cu–Ni–Zn couples as function of composition with Profiler. Campbell et al. [44] investigated multicomponent diffusion between two Ni-base superalloys with DICTRA, based on the diffusion mobility database developed for the multicomponent Ni solid solution [45]. Another method for obtaining the coefficients of the diffusivity matrix from diffusion couple measurements is the least-square procedure proposed by Miller [46] for the case of constant diffusivities, i.e. independent of composition.

Although several methods for determining the diffusivity matrix from experimental data are available, no experiments on diffusion in ternary metallic liquids have been reported to our best knowledge and none addressed quaternary or higher order liquids. The investigated ternary liquids are mainly transparent materials and the measurements are performed by Rayleigh interferometry, that takes advantage of the refractive index changing with composition. Some experiments on ternary molten salts are reported as well. The lack of diffusion experiments in liquid metallic alloys is mainly due to the fact, that even low velocities of convective fluid flow change diffusive transport into convecto-diffusive transport. Up to now, the best method to avoid buoyancy driven convection is to perform diffusivity measurements in microgravity using the sheer cell technique, as discussed by Praisey [47], and Frohberg et al. [48]. Recently Garandet et al. [49] and Botton et al. [50] proposed an alternative to microgravity experiments for electrically conducting liquids based on magnetohydrodynamic (MHD) damping of fluid flow in a uniform magnetic field. The strategy is to perform diffusion experiments with sheer cells with different values of the magnetic field and to extrapolate the apparent diffusivities to the case of an infinite magnetic field. The key is a model of diffusion in the presence of MHD-damped convection. Experiments performed for Sn–SnIn 1 at.% and Sn–SnIn 0.5 at.% [50] showed promising results. Application of this method to multicomponent liquids opens up new perspectives. Until then, it is useful to work with diffusion coefficients taken from binary alloys as diagonal terms of the diffusivity matrix or else to take advantage of DICTRA's capability to construct diffusion mobility databases by extrapolating form already assessed lower order systems.

3.2. Interfacial energies

The thermophysical properties of an interface established between two homogeneous bulk phases in equilibrium result from the fact that the atoms at the interface are situated in a different environment than inside the bulk phases. An interface is thus associated with free energy and entropy that reflect the local, atomistic scale structure of the interface.

Direct experimental measurement of the interfacial free energy is beyond reach, but indirect techniques have been developed, that take advantage of the fact that measurable quantities sensitively depend on the interfacial free energy. Comprehensive reviews of these techniques are due to Woodruff [51], Eustathopoulos [52] and Kelton [53]. Most of the experiments were dedicated to pure materials and binary alloys and only few to ternary alloys. Vahlas et al. [54] performed experiments on ternary Al–Sn–In and Zn–Pb–Sn alloys in order to check pair interaction models on the influence of concentration and temperature on both, adsorption and interface structure. Ongoing work on ternary alloys, however, is based on the grain boundary groove technique applied by Gündüz and Hunt [55] and Maraşli and Hunt [56] to binary alloys in eutectic and peritectic equilibrium. The method has been used to determine both, the solid/liquid interfacial free energy from the Gibbs–Thomson coefficient and the interfacial free energy of solid/solid hetero-interfaces from force equilibrium at the triple

junction. Grain boundary groove techniques may potentially be a very sensitive method also for determining the anisotropy of the interfacial energy, as pointed out by Voorhees et al. [57] and Napolitano [58].

Among the computational methods for determination of the equilibrium properties of solid/liquid and solid/solid interfaces atomistic simulation methods emerged as very promising. In a recent review Hoyt et al. [59] described molecular dynamics and Monte Carlo simulation methods applied to characterize solid/liquid interfaces in unary and binary alloys. They pointed out that the most important contribution of atomistic simulations relays in their capability of accurately determining even small values of the crystalline anisotropy of the solid/liquid interfacial energy. Atomistic simulations proved to be very effective also in predicting equilibrium interfacial adsorption. Appreciable adsorption would imply non-trivial composition dependencies of the interfacial energy. Molecular dynamic simulations by Sibug-Aga and Laird [60] and Davidchack and Laird [61] for binary hard-sphere mixtures found no evidence for significant adsorption at solid/liquid interfaces. For ternary alloys the question of equilibrium interfacial adsorption is more complex, because two independent composition profiles that minimize interfacial energy need to be determined.

To our knowledge this has not been investigated for solid/liquid interfaces, yet. For solid/solid interfaces in dilute ternary alloys however, several interesting results have been reported: Kooi [62] discussed the equilibrium adsorption at coherent (1 0 0) interfaces in ternary face centered cubic systems analyzed using the cluster variation method in comparison to the regular solution model by Dreggia and Wynblatt [63]. Zhang et al. [64] used the Monte Carlo simulation technique in junction with the embedded atom method to model the composition and structure of semi-coherent (1 1 1) and (0 0 1) hetero-interfaces in Ni–Ag–Cu alloys. Significant adsorption of Cu was reported for both orientations. The (0 0 1) orientation was found to show a tendency for faceting, with adsorption of Cu tending to stabilize certain facets against other. This brief outline of atomistic simulations is just meant to encourage the reader to think of them as future powerful tools also for ternary and multicomponent alloys.

Field theoretical methods have been used extensively to address interfaces in binary, ternary and three-phase systems. While a large number of works address the related problems, due to space limitations, we mention here only a few representative studies. Molecular theory based on the density functional technique [65] and Cahn–Hilliard type calculations [66] indicate that the metastable crystalline phases may ‘wet’ the interface between the stable solid and liquid (creating an interfacial layer of the metastable phase between the stable phases), reducing thus the interface free energy. Multi-component interfaces appearing in phase separating systems have been investigated within the framework of the Cahn–Hilliard theory. Hoyt [67] formulated a general approach, and reported a linear variation of the interface free energy with the addition of a small amount of a third ideal component to binaries. Huang et al. [68] studied surface adsorption in ternary phase separating systems, and found that in symmetrical ternaries, the surface adsorption of the minority component depends strongly on the magnitude of the respective square-gradient term. The phase field theory, an approach able to describe structural changes at the interface, (see Sections 5 and 6.2) has been used widely to address solid/liquid and solid/solid interfaces in binary systems, e.g. [69,70]. For example, the free energy of a binary solid/liquid interface of an ideal solution interpolates linearly between the pure components as a function of temperature, provided that the physical interface thickness and a single gradient term are used (for the phase field). In the presence of a gradient term for the concentration field, surface adsorption is observed, and a maximum in the interface free energy occurs as a function of temperature [69]. Although molecular theories based on the density functional technique have been used extensively to study binary vapor/liquid and liquid/liquid interfaces, only a few works are relevant to the binary solid/liquid interface (binary liquid at hard wall, see e.g. [71]).

A last issue we wish to mention here, regards the multiphase or composite interfaces that form when two or several phases simultaneously grow from the liquid, e.g. in eutectic reaction. It is useful to assign an integral or effective value of the interfacial free energy to a composite interface, in order to assess the shift of the average interface temperature related to curvatures much larger than the phase spacings. Plapp and Karma [72] derived an expression for the Gibbs-Thomson coefficient of a 2D lamellar eutectic interface, which is a function of the volume fractions of the phases, their individual Gibbs-Thomson coefficients and the contact angles established at the triple points. It is obvious that in 3D the effective interfacial energy of a lamellar composite interface will be anisotropic, even when each phase is isotropic. This anisotropy results from the lamellar arrangement itself, or more generally from the geometry of the multiphase pattern. Purely topologic anisotropy, but also its relation to crystalline anisotropy, seem to constitute interesting topics for future research.

4. Microstructure evolution during solidification

Microstructure evolution during multiphase solidification of multicomponent alloys encompasses several aspects that are most easily dealt with, when dividing the topic into three subsections: First (Section 4.1), we discuss the stability and dynamic behavior of morphological patterns at a multiphase, or ''composite'' solid/liquid interface that exhibits steady state coupled growth of non-faceted phases. Coupled growth morphologies compete with other, non-coupled morphological patterns, an issue that we briefly discuss in Section 4.2 within the frame of microstructure selection maps. Last but not least, we address multiphase microstructures that evolve in successive reactions along the solidification path of multicomponent alloys (Section 4.3). Investigations into this latter area are strongly driven by industrial demand. Assessing all the achievements is beyond reach and we will only point out the potential of selected experimental and computational tools for application purposes.

4.1. Coupled growth in bulk (3D) and thin (2D) samples

Coupled growth of two distinct phases from a binary liquid in eutectic [73–76] and monotectic [77–81] reaction attracted much attention since the periodic patterns evolving at the solid/liquid interface exhibit rich dynamics with regard to their spatio-temporal evolution. Coupled growth in peritectic reaction has been a subject of controversial discussion but recently both experiments and simulations [81,82] showed, that it can be achieved under specific growth conditions.

Most of the work on coupled growth is performed for steady state unidirectional solidification in merely diffusive growth conditions. Such conditions can be achieved experimentally in the Bridgman–Stockbarger process for alloys with thermo-solutally stable density profiles. This process can be equally applied to bulk samples (3D) and thin samples (quasi 2D). The first is typically dedicated to metallic alloys, the latter to transparent organic alloys that are fully analogous to metals as far as solidification is concerned. With transparent organic alloys it is possible to follow the spatio-temporal evolution of the microstructure in real time with an optical microscope. This possibility obviously is of crucial importance for really identifying the mechanisms at play knowing their fully out-of-equilibrium nature. Recent improvements in the experimental method and in the methods of numerical simulation have allowed important steps forward to be made. For binary eutectics, our understanding of the dynamics of 2D lamellar eutectics is practically complete [84–88]. Latest developments focus

on extending the use of transparent binary eutectic alloys to 3D growth configurations and on using low melting point metallic alloys in 2D growth configurations with real time observation under an optical microscope in reflection.

The availability of 2D and 3D experimental techniques proves to be all the more important when looking at coupled growth in multicomponent alloys. For the case of coupled eutectic growth in ternary alloys we will show that for both univariant and nonvariant eutectic reactions specific features of morphological instability and pattern formation are related to 3D. Our restriction to ternary eutectic growth is due to the fact that quasi-peritectic and peritectic growth in ternary alloys has not yet been investigated in detail, at least to our knowledge and work on monotectic growth in ternary alloys is quite limited as well (see Section 4.2). Ternary eutectic growth, however, raised vivid interest since the 1960 and early 1970. The additional degree of freedom associated to the univariant eutectic reaction was expected to render two-phase aligned microstructures in an easy to control solidification process. Driven by this objective, univariant eutectic growth was investigated in several ternary eutectic alloys [89–92] but also in multicomponent alloys. Another goal was to enhance properties of lamellar eutectic microstructures by in situ fiber reinforcement, thus looking for nonvariant ternary eutectics with the third phase forming well dispersed fibers within the lamellar pattern of the other two phases. Driven by this objective, nonvariant coupled growth was investigated in several ternary alloy systems [92–95] and the obtained patterns were characterized in terms of volume fractions of the three phases, the pattern type and eutectic spacings.

4.1.1. Coupled growth and morphological stability of univariant eutectics

In univariant eutectic reaction coupled growth of two non-faceted solid phases from the ternary liquid results in a regular lamellar or rod-like arrangement of the phases. They grow with an interlamellar exchange of solute species but additionally segregate the third component into the liquid, such that a long-range solute boundary layer establishes in the liquid ahead of the interface. When the steady state growth velocity approaches zero, the composition of the phases in equilibrium at the interface is given by the tie triangle that exactly contains the overall composition of the alloy on its solid–solid tie line (see Fig. 10).

McCartney, Jordan and Hunt [97,98] were the first to extend the Jackson–Hunt theory for binary alloys [73] to univariant eutectics. They derived an expression for the relationship between interface undercooling, growth velocity and eutectic spacing, that for minimum undercooling yields $\lambda^2 v = K$. For calculation of the constant K the materials properties i.e. thermodynamic data, diffusion and interface energies need to be available for the ternary alloy, which makes this a difficult task. A similar expression was proposed by De Wilde et al. [99], who discussed the sensitivity of the constant K relative to the input data. Experiments confirmed the $\lambda^2 v = K$ relationship both for rod-like eutectic in Fe–Si–Mn and Fe–Si–Co as shown by Yamauchi et al. [100] and for lamellar eutectics in Al–Cu–Ni by Rinaldi et al. [95] Al–Cu–Ag by De Wilde et al. [99] and Ni–Al–Cr–Mo by Raj and Locci [101].

The planar interface of a univariant eutectic is however prone to morphological instabilities due to the long-range solute boundary layer established in the liquid ahead of the interface. Fig. 12a through d depicts the solutal configuration obtained at the planar eutectic interface in the ternary alloy Al–Cu 15.52 at.%–Ag 9.04 at.% after unidirectional solidification and subsequent quenching of the bulk sample according to Hecht et al. [102]. Qualitatively this configuration is similar to what is known from the single-phase solidification of a binary alloy with a planar solid/liquid interface, which of course is also univariant.

Rinaldi et al. [95] and McCartney et al. [97] proposed a constitutional supercooling criterion for defining the stability limit for planar univariant eutectic growth, by assuming that a Mullins–Sekerka (MS) type instability applies for the transition from planar to cellular eutectic growth. The constitu-

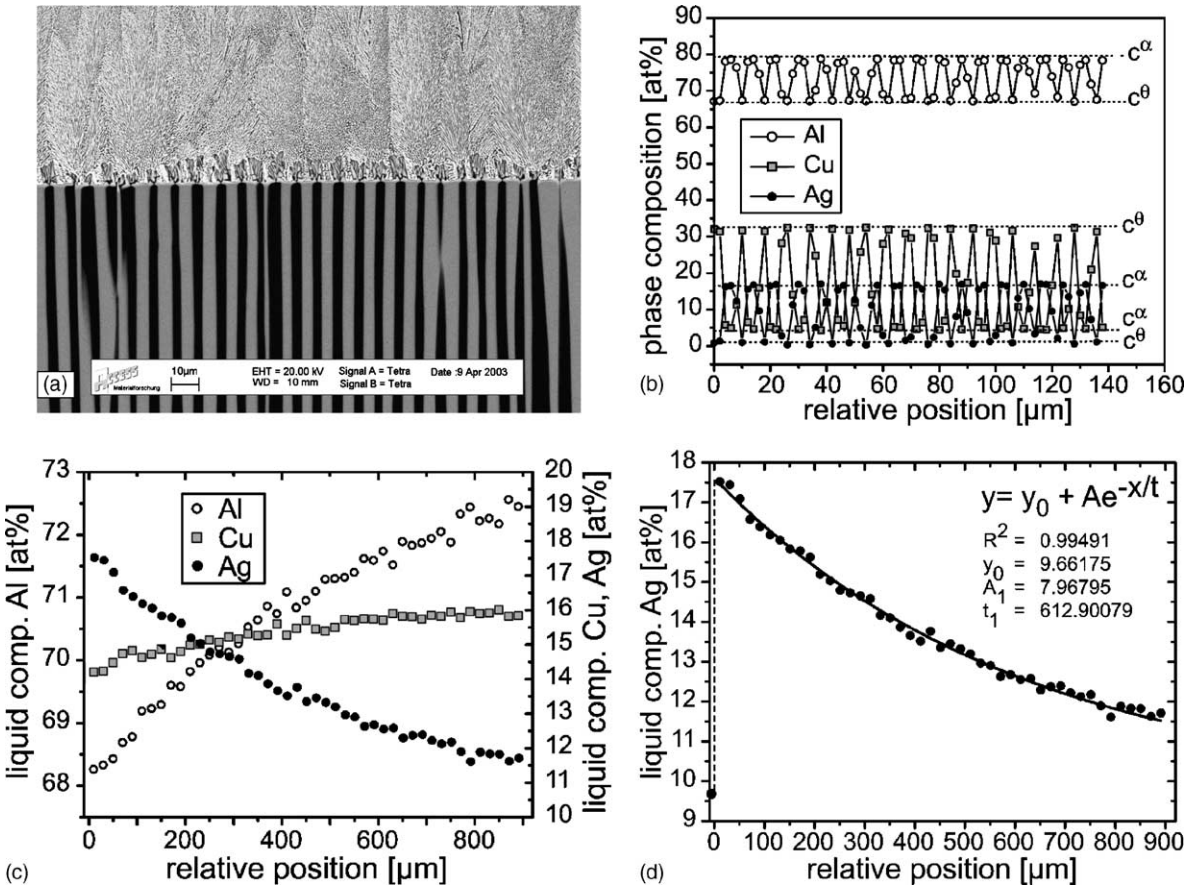

Fig. 12. Solutal configuration at a planar eutectic interface during steady state growth in the ternary alloy Al–Cu 15.52 at.%–Ag 9.04 at.% after unidirectional solidification with a velocity $v = 1.417 \times 10^{-6}$ m/s in a temperature gradient $G = 27 \times 10^3$ K/m: (a) quenched interface in longitudinal section, with Al_2Cu (θ-phase) black and α(Al) light grey, (b) element distribution in the solid across the eutectic lamellae measured by EDX, (c) element distribution in the liquid ahead of the quenched interface (d) exponential fit of the Ag distribution profile ahead of the quenched interface. The Ag content of the solid (phase fraction weighted) is given at the position $z = -5$ µm.

tional supercooling criterion can then be formulated in terms of the third, segregating component ''C'' [95]:

$$\frac{G}{v} = \frac{M_C}{D_C}\left(1 - \frac{1}{k_C}\right) c_{\infty C} \tag{12}$$

where G/v is the stability limit for planar eutectic growth, with G the temperature gradient, v the growth velocity, D_C the diffusion coefficient of component ''C'', M_C the slope of the univariant eutectic groove, k_C the phase fraction weighted eutectic distribution coefficient for component ''C'' and $c_{\infty C}$ the initial concentration of component ''C'' in the alloy.

When applied to the alloy Al–Cu 15.52 at.%–Ag 9.04 at.% considered above, with the data summarized in Table 4, the critical velocity equals 1.67×10^{-6} m/s.

For an estimation of the stability limit for different alloys along the eutectic groove liquid → α(Al) + Al_2Cu in the ternary alloy system Al–Cu–Ag one can apply Eq. (12) based on the thermodynamic data presented in Section 2, Tables 2 and 3, moreover assuming that the effective diffusion coefficient of Ag is independent of the overall alloy composition.

Table 4
Material data used for calculation of the critical velocity of MS instability onset for Al–Cu 15.52 at.%–Ag 9.04 at.%

Property	Unit	Value	Source
$c_{\infty Ag}$	at.%	9.04	Chemical analysis
k_{Ag}	–	0.54	Thermodynamic calculations
M_{Ag}	K/at.%	−1.8	Thermodynamic calculations
D_{Ag}	m^2/s	0.89×10^{-9}	Fit of the measured Ag-profile (Fig. 12d)
G	K/m	27×10^3	Process data

Fig. 13a shows the calculated velocities of instability onset for the thermal gradient $G = 27 \times 10^3$ K/m for alloy compositions exactly on groove and for alloy compositions that are 2% of groove, but still on the tie lines, as depicted in Fig. 13b. Experimentally observed transitions from planar and cellular growth structures fit quite well to the obtained transition criteria.

This approach of an impurity driven Mullins–Sekerka instability, similar to that for a single-phase solid, leaves aside the most interesting aspect of morphological destabilization of a planar eutectic interface, namely the interplay between the eutectic pattern and the instability.

The first attempt to analyze the stability of a lamellar eutectic interface in the presence of a low content of a ternary impurity (dilute limit) is due to Plapp and Karma [72]. They extended Datye and Langer's linear stability analysis [103] to a ternary eutectic groove in the vicinity of a binary eutectic point, with all slopes being constant and the solubility of the solid phases being independent of temperature. The analysis provides the full linear stability spectrum of the steady state lamellar eutectic front in 2D. From studying the stability for an alloy of eutectic (on-groove) composition with a symmetric phase diagram, Plapp and Karma concluded that:

a) The primary instability of the eutectic interface is qualitatively similar to the Mullins–Sekerka (MS) instability of a monophase interface in binary alloys.

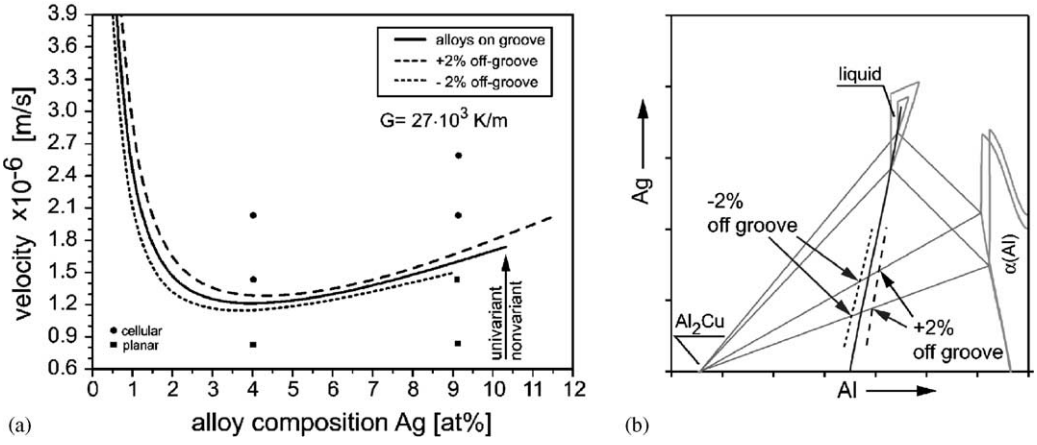

Fig. 13. (a) Calculated velocities for instability onset for ternary Al–Cu–Ag alloys along the univariant eutectic groove: liquid → α(Al) + Al_2Cu based on Eq. (12) and the thermodynamic data presented in Tables 2 and 3. The calculations were done for alloys with exactly on-groove composition and alloys that are 2% off-grove towards the Al-rich side (red) and the Cu-rich side (green), respectively. The scheme in panel (b) illustrates this. The alloys more rich in Al grow with higher fractions of the Ag-rich α(Al) and thus segregation of Ag is less pronounced. Consequently they are more stable. The reverse holds for alloys that are more rich in Cu.

b) Additional to the standard MS, two stabilizing terms occur in the expressions for the critical velocity and the critical wave number at onset: They are identified as contributions to an effective capillary length due to (i) the surface tension of the eutectic interface consisting of an array of arcs and to (ii) the eutectic cross-diffusion, that acts as a capillary force. These terms become significant for very small concentrations of the ternary impurity.
c) Oscillatory modes with long-wavelength originate in a transient regime. They are due to the interplay between the MS instability and the resulting local changes of the eutectic spacings.

The formation of eutectic cells (colonies) in the binary organic eutectic CBr_4–C_2Cl_6 doped with different low concentration of naphthalene, ranging from 2.5×10^{-2} to 1×10^{-1} at.% has been recently studied by Akamatsu and Faivre [104] in thin samples. For high impurity concentrations travelling waves were found to occur prior to the formation of cells and that local two-phase structures (fingers) are intermediate to cell formation. More, no steady state pattern was reached on the scale of individual cells, suggesting that cells were intrinsically unsteady, an observation that was perhaps due to the low anisotropy of the interfacial properties. Fig. 14 shows two snapshots of the eutectic interface in CBr_4–C_2Cl_6–naphthalene with 5×10^{-2} at.% of naphthalene, obtained during directional solidification of a 12 μm-thick sample.

In bulk samples, additional phenomena arise from the 3D nature of the eutectic and the cellular pattern: Based on unidirectional solidification experiments with different Al–Cu–Ag alloys with Ag concentration ranging from 4 to 10 at.% Hecht et al. [102] argued that the primary instability of an initially planar eutectic interface consisting of α(Al) and Al_2Cu lamellae occurred within the plane of the lamellae rather than in direction perpendicular to the lamellae.

This inherently 3D-process leads to the formation of elongated cells that only in a later step were found to break down to regular cells. The transition form elongated to regular cells was shown to be associated to a complex fragmentation of the lamellar structure and was found to occur more or less easy, depending on the grains inside the multigrain alloys. Elongated cells, as precursors to regular cells and fully developed regular cells, are shown in sections perpendicular to the growth direction in Fig. 15a and b. A similar process of cell formation was observed by De Wilde for eutectic growth of α(Al) and Al_2Cu lamellae in ternary Al–Cu–Si alloys. This specific break-up process may be due to the significant difference between the solid/liquid surface energy of α(Al) and the Al_2Cu phase, as measured in binary Al–Cu alloys by Gündüz and Hunt [55] and Maraşli and Hunt [56]. In this sense,

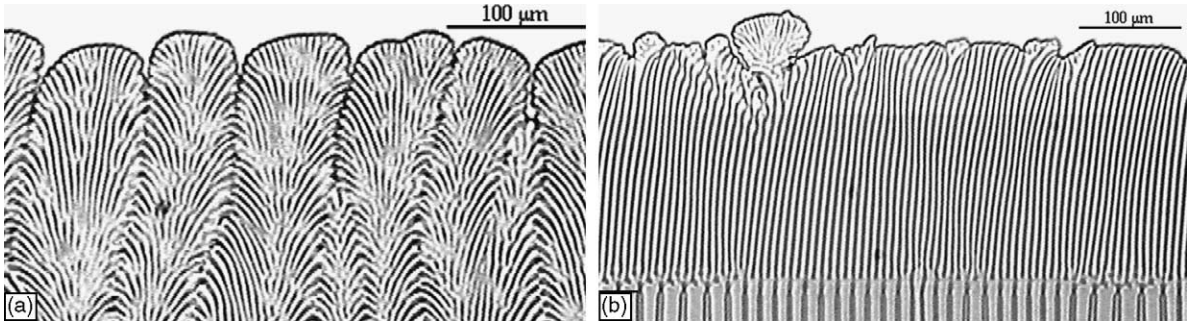

Fig. 14. The quasi-2D cellular pattern (a) obtained for $v = 31 \times 10^{-6}$ m/s and $G = 110 \times 10^2$ K/m shows a chaotic behavior, comparable to that of single phase cells in dilute alloys when interfacial anisotropy is weak. The transient that led to this pattern is depicted in (b), corresponding to a switch of the pulling velocity from 0.9×10^{-6} to 31×10^{-6} m/s. The initially stable lamellar eutectic interface goes through a series of complex processes (branching, traveling waves, two-phase fingers). The coupling between the interlamellar and the cellular dynamics clearly results in an overstabilisation of the lamellar front, which is only destroyed when two phases fingers appear.

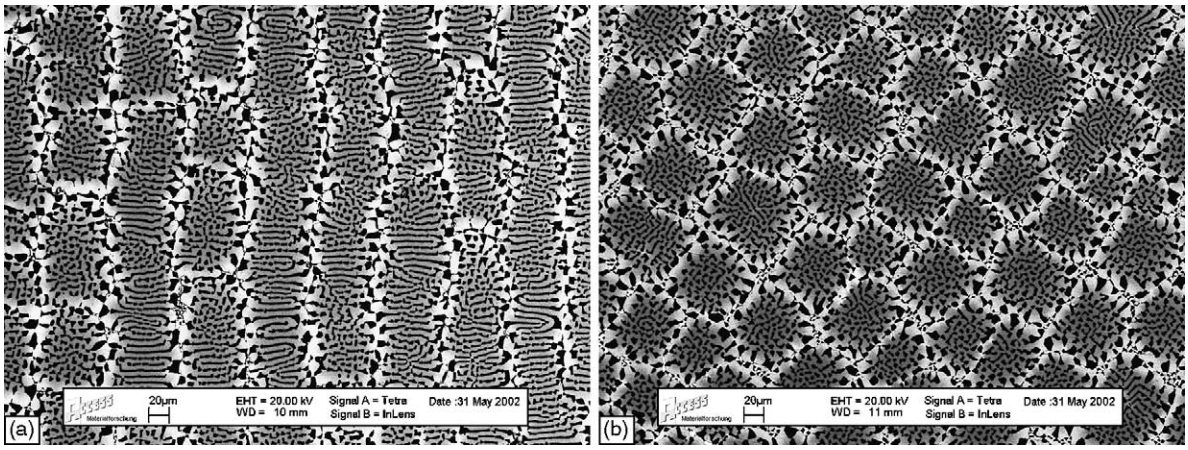

Fig. 15. Cross section through an array of elongated cells (a) in Al–Cu 13.66 at.%–Ag 10.27 at.% solidified at $v = 2.033 \times 10^{-6}$ m/s and $G = 27 \times 10^{3}$ K/m. At several places inside the elongated cells, regular cells with square-like shape can be observed in various states of maturity. Cross section through an array of regular cells (b) in Al–Cu 13.66 at.%–Ag 10.27 at.% solidified at $v = 2.6 \times 10^{-6}$ m/s and $G = 27 \times 10^{3}$ K/m. The order of the pattern is quadratic [102] with the average cell spacing about one order of magnitude larger then the eutectic spacing prior to destabilization. The diffusion length $l_D = D_{Ag}/v$ ranges at about 340 μm.

the lower interfacial energy of Al_2Cu/liquid interfaces may ease the instability along Al_2Cu-lamellea which, as a leading phase, induce a coupled instability along the α(Al)-lamellae as well. This effect may be enhanced by the interlamellar diffusion that stabilizes the interface in direction perpendicular to the lamellae, as pointed out above. Also the 3D topologic anisotropy of a lamellar eutectic interface in conjunction with the crystalline anisotropy of the Al_2Cu-phase may play the decisive role. The existence of elongated cells as precursors to regular cells has been observed for monophase solidification by Morris and Winegard [105] for binary Pb–Sb alloys. For the [110] axis of the growing solid solution aligned in the direction of growth, elongated cells were reported, while for [100] and [111] orientations regular cells formed directly. This implies that anisotropy is an important factor that effectively governs details of the destabilization process and of the stability of the resulting cellular structure.

The role of topologic and crystalline anisotropy for the stability of cellular patterns, the order of the patterns and the shape of individual cells inside the pattern is an issue of further interest. Experimentally observed cellular patterns in other alloy systems including intermetallics [101] and ceramics [6] strongly point in this direction.

4.1.2. Coupled growth of nonvariant eutectics

In nonvariant eutectic reaction three solid phases can simultaneously grow from the ternary liquid alloy by exchanging solute species in diffusion perpendicular to the growth direction. The composition of the phases in equilibrium at the interface and the mole fraction of the phases is given by the tie triangle corresponding to the temperature of the nonvariant eutectic point. For practical situations the tie triangle is not equilateral, i.e. the phase diagram is not symmetrical. Therefore, even when assuming equal surface energies for all hetero-interfaces in the system, the eutectic pattern selected by the system will be the one that minimizes diffusion paths. This means that the two solid phases joined by the hypotenuse of the tie triangle will tend to exhibit smaller mutual distances compared to the others. Except for the ideal lamellar pattern expected to form for a symmetric phase diagram, and observed in Cd–Sn–Pb by Kerr et al. [106] and Bao and Durand [96] all experimentally observed three-phase patterns show periodic arrangements of duplex structures that exhibit quadruple points in

addition to triple lines. Cooksey and Hellawell [93] discussed possible patterns produced by the interplay of solute diffusion and the energy of hetero-interfaces based on experimental observations of bulk samples for different alloys from the ternary systems Cd–Sn–(Pb, In, Tl), Al–Cu–(Mg, Zn, Al) and Zn–Sn–Pb. Except for Cd–Sn–Pb all observed patterns exhibited quadruple points.

Experiments on different ternary eutectics by Holder and Oliver [107], Rinaldi et al. [95], Rios et al. [108] and Ruggiero and Rutter [109] showed, that the three-phase patterns generally obey a $\lambda^2 v = K$ relationship for each pair of phases. Recently Himemiya and Umeda [110] published three phase eutectic growth models for the ideal lamellar pattern and constructed ''rod + hexagon'' and ''semiregular brick type'' patterns, following the procedure applied by Jackson and Hunt for binary eutectics. The models were applied to coupled growth in Sn–Pb–Cd and Al–Cu–Ag ternary eutectic alloys: For both alloys the computed interface undercooling versus growth rate was lowest for the rod + hexagon pattern and highest for the ideal lamellar pattern.

Many more questions are still open, regarding the spatio-temporal evolution of three-phase ternary eutectic patterns. From the above described aspects related to pattern selection, it emerges as challenging to question what coupled growth patterns will select, when forcing the alloy to grow in a 2D-confinement, i.e. when prohibiting the formation of quadruple points. In this regard comparative 2D and 3D investigations of pattern selection and its spatio-temporal evolution will be the method of choice for future work. On the experimental side much progress is expected from two recent developments: Witusiewicz et al. [111] and Sturz et al. [112] proposed a quaternary organic eutectic alloy system for in situ investigations. The alloy system is succinonitrile (SCN) — neopenthylglycole (NPG)—(D)camphor—amino-methyl-propanediol (AMP). At small additions AMP dissolves mainly in NPG, such that a three-phase eutectic consisting of SCN—NPG—(D)Caphor is achieved, with all three phases being non-faceted. With such a system available, in situ observation techniques in 2D and 3D will allow to gain more insight into all questions of pattern formation and stability. Growth of metallic ternary eutectics in flat glass samples are presently being studied in the system In–Bi–Sn with in situ observation under a microscope in reflection. Naturally eutectic In–Bi–Sn alloys can also be processed as bulk samples in the classical Bridgman furnace as well. This opens up the possibility to compare 2D with 3D growth also in metallic alloys.

Apel et al. [113] recently presented phase field simulations of the ternary Al–Cu–Ag eutectic for different stacking sequences of the three phases Ag_2Al = A, Al_2Cu = B and α(Al) = C. For stacking sequences ABC no axisymmetric lamellar pattern was found, but the lamellae were slightly tilted relative to the growth direction. In contrast to tilted growth modes in binary alloys the tilted growth here was a direct consequence of the lack of mirror symmetry in the ABC stacking sequence. Higher order sequences with mirror symmetry, e.g. BACBC and BCACBC were shown to accomplish axisymmetric growth. For the same periodic length these sequences were shown to correspond to different undercoolings. More details will be given in Section 5.3. A first 3D simulation qualitatively reproduces experimentally observed quadruple points and duplex structures, as shown in Fig. 16.

4.1.3. Fluid flow effects on coupled growth

Coupled growth in nonvariant eutectic and monotectic reaction leads to a periodic concentration profile in the liquid close to the interface that decays in direction perpendicular to the interface much faster than in single phase solidification. The characteristic length is not D_i/v, but the lamellar or fiber spacing itself. Therefore the effects of buoyancy induced convection on nonvariant coupled growth structures are rather small, provided that the alloy composition is exactly corresponding to the nonvariant point, the phase diagram is symmetric and all phases have the same interface kinetics. In addition to buoyancy, fluid flow can be induced by density differences between the growing phases and, specifically relevant to monotectics, by thermocapillary effects. In what follows we discuss the

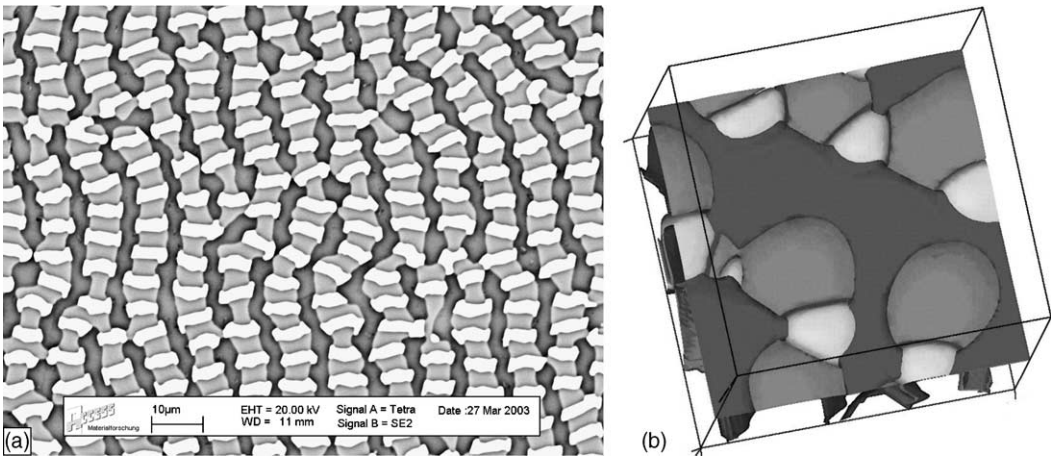

Fig. 16. Cross section through the three-phase eutectic pattern of the ternary alloy Al–Cu 13 at.%–Ag 17 at.% after unidirectional solidification in a temperature gradient $G \approx 27 \times 10^3$ K/m with a velocity $v = 1.42 \times 10^{-6}$ m/s (a) and snapshot of the three-phase eutectic pattern obtained for a 3D simulation for $G = 5 \times 10^3$ K/m and $v = 0.5 \times 10^{-6}$ m/s (b). For both images (a) and (b), the phases are Ag_2Al—white, Al_2Cu—light grey, α(Al)—dark grey.

effects of fluid flow on eutectic alloys and monotectic alloys. The discussion refers mainly to binary alloys. For univariant or nonvariant coupled growth in ternary alloys both experiments and models dedicated to the effect of fluid flow remain challenges to future work.

For binary eutectic Al–Si alloys Sens et al. [114] verified that different interface kinetics of the two phases in eutectic growth leads to a significant departure of the average composition of the liquid at the solid/liquid interface from the eutectic nonvariant composition. The authors showed, that adsorption of Sr at the solid/liquid interface of Si causes an increase of the kinetic undercooling for the growth of this phase. Simultaneously, the average liquid composition is shifted towards values richer in Si. Fluid flow due to buoyancy effects is then no longer negligible.

The effect of buoyancy driven convection on eutectic structures was investigated many times, especially since the availability of solidification processing under microgravity conditions. An example of this type of investigations is shown in Fig. 17a summarizing the results of different experiments for coupled eutectic growth of Al-Ni alloys reported by Buchholz and Ratke [115], Favier and De Goer [116], Lemkey [117] and Barczy [118]. Interesting is, that although each author verified

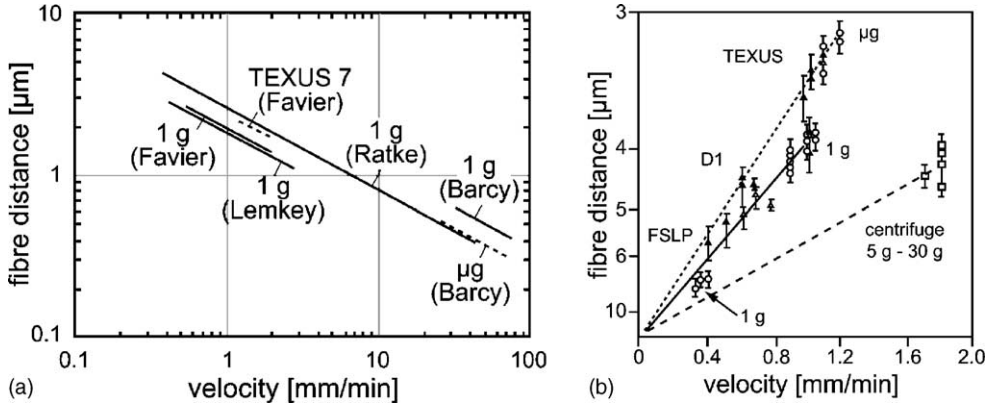

Fig. 17. Effects of fluid flow on the average fibre distance in rod-like binary Ni–Al eutectic (a) and quasi-binary InSb–NiSb eutectic (b).

the Jackson and Hunt relationship, the values of the constant K_{JH} seem to differ by at least a factor of two and even the results obtained under microgravity conditions, which should not be influenced by parasitic fluid flow effects, differ significantly. Fig. 17b reproduces the experimental results of Müller and Kyr [119] obtained for coupled growth of the quasi-binary eutectic InSb–NiSb in the ternary alloy system In–Sb–Ni. The spacings on earth and in space in quasi-binary InSb–NiSb eutectics depend strongly on gravity.

The effects of buoyancy induced fluid flow on coupled growth of eutectics remains unresolved. Favier et al. [116] explained the different effects of fluid flow observed in Ni–Al eutectics, as stemming from a deviation relative to the exact eutectic composition and derived how much deviation is necessary to observe such effects. This approach was questioned by several authors [118,119]. Drevet et al. [120], however, showed that convectively induced segregation at the solid/liquid interface of slightly off-eutectic alloys leads to a decrease of spacings.

In the past decade no new experimental results were reported, either in reduced gravity nor on earth using for instance artificial fluid flow induced by electromagnetic stirring to modify mass transport in a controlled way. In recent, unpublished work on eutectic growth in ternary Al–Si–Mg alloys Steinbach [121] observed that rotating magnenetic fields and the fluid flow induced by them change the eutectic spacing: The larger the flow velocity the smaller the spacing. Fitting the measured spacings with a Jackson–Hunt relation $K_{JH} = \lambda^2 v$, yields that the constant K_{JH} depends linearly on the flow velocity.

A theoretical approach to understand the effect of flow has been performed by Ma et al. [122]. They analyzed a flow field parallel to the interface having a constant velocity gradient γ in direction perpendicular to the interface. Performing a classical Jackson and Hunt analysis they derived the relation

$$\lambda_E = \lambda_{E0}\left(1 - \frac{2D\gamma}{v^2}\right)^{0.5} \tag{13}$$

with D the diffusion coefficient, v the growth velocity, λ_{E0} the spacing without flow and λ_E the spacing with flow. Qualitatively the theory predicts a decreasing spacing with increasing fluid flow and also fits to the data of Steinbach. Concluding, the effect of buoyancy induced fluid flow on eutectic spacing needs much more experimental and theoretical research before any definitive conclusion can be drawn.

Flow induced by density differences between the phases is not directly tractable by experiments, but relies on comparing experimentally observed eutectic spacings with those predicted from the Jackson–Hunt theory. In its original formulation [73] the Jackson–Hunt theory on spacing selection for coupled growth was formulated for equal density of all phases. Several approximations were proposed as to include the density differences and the resulting flow into JH-models, by Magnin and Trivedi [123], Kim et al. [124] and Coriell at al. [80]. The problem is not trivial, because the growing phases generally have different densities, each being different form the density of the liquid. Accordingly, the flow has components both perpendicular and transverse to the solid/liquid interface. Recently Coriell et al. [125] proposed a numerical solution to the problem by solving the Navier–Stokes equation in the Stokes flow approximation and introducing the corresponding advective terms into the equation for solute diffusion that enters the JH-analysis. The authors discussed the numerical results in comparison to the modified JH-Model [80] for eutectic growth of tin-lead and iron-carbon, but also for monotectic growth of aluminum-indium.

For monotectic growth the effects of fluid flow are even more significant, since one of the phases growing in monotectic reaction from liquid L_1 is a liquid phase as well as L_2. The L_1/L_2 interface will

be a low energy interface with high mobility that represents a high diffusivity path. Generally, the monotectic composition is low and close to the higher melting point component, such that the L_2 phase, minimizes its interfacial energy to the growing solid phase by taking a rod-like shape [117]. Ratke and co-workers [81,126,127] introduced the idea, that the thermocapillary effect at the L_1/L_2 interface causes Marangoni convection. This induces a flow vortex and has an influence on the solute transport and thus the constitutional supercooling of the solidification front. They developed an analytical theory and a numerical model. With both they could show that a new relation between the fibre distance $2R$ and the solidification velocity v should be observable. At small temperature gradients a Jackson and Hunt type relation should hold, but with increasing temperature gradient the fibre spacing should increase at constant solidification velocity. A few experimental results, reported by Kamino et al. [78], for monotectic growth in Al–In fall into the range of numerically calculated data, as shown in Fig. 18. Although this theory of monotectic coupled growth in which interface convection plays a dominant role might be questioned and is not validated experimentally, it points out the importance of convective mass transport on microstructure evolution.

Few investigations on monotectic growth in ternary alloys have been reported: Andrews et al. [130] tested the influence of convection on hypermonotectic samples in ternary Cu–Pb–Al alloys. Unidirectionally solidification experiments were performed aboard NASA's KC-135 zero-g aircraft during cyclic gravity-level variations consisting of approximately 25 s at 0.01 g followed by approximately 45 s at 1.8 g on board KC-135. In the ternary phase diagram Cu–Al–Pb, both Al–Pb and Cu–Pb exhibit a miscibility gap. Thus in the ternary system a miscibility volume with a large binodal surface exists. Along this surface the liquid–liquid interface tension drastically changes with serious consequences on phase decomposition kinetics and fluid flow (Marangoni convection). The metallographic analysis of the samples after flight clearly showed aligned growth during the reduced gravity level periods and a dispersed structure in the high-g periods. This is in contrast to experiments performed by Dhindaw et al. [131] using upward unidirectional solidification at different rates to study the effects of gravity level binary Cu–Pb and Bi–Ga alloys on board a KC-135 airplane. They found that coupled growth was favored by a high gravity level and that a dispersed microstructure was formed in the solid, whenever growth began in a low gravity cycle.

Summarizing, one may conclude that the effect of fluid flow driven by buoyancy, density differences and capillary effects on coupled growth of binary eutectic and monotectic alloys is not

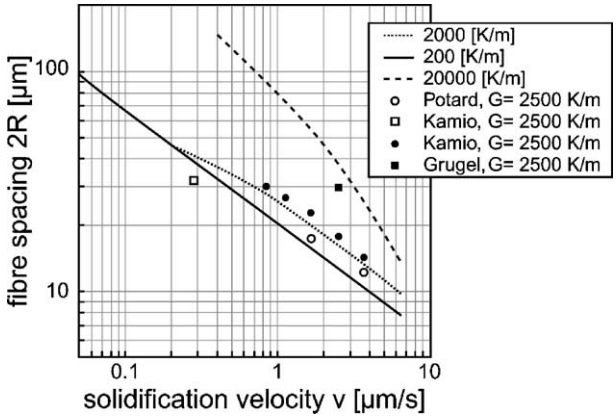

Fig. 18. Jackson and Hunt diagram for different temperature gradients as calculated with the numerical model of Stöcker and Ratke [126,127]. The calculations were performed with the materials' parameters for monotectic Al–In alloys. Experimental data from Kamino et al. [78], Grugel [128] and Potard [129] are given for comparison.

fully understood, today. For ternary univariant and nonvariant alloys investigations into this area pertain to future.

4.2. Microstructure selection maps

For most application purposes, detailed information about local microstructural features is less important then knowledge of the types of microstructure and the transition thresholds between the different types as function of alloy composition and processing conditions. Microstructure selection maps emerged as a highly integrated, yet easy to read way of representing exactly this kind of information. They comprise the results of experiments or microstructure modelling for a large spectrum of alloy compositions and solidification conditions. In the recent review article ''Solidification microstructures: Recent developments, future directions'' Boettinger et al. [132] described the progress in the area of phase and microstructure selection for nucleation controlled, growth-controlled and mixed processes with reference to binary alloy systems. Gilgien and Kurz [133] summarized the methodology of constructing microstructure selection maps for rapid solidification of binary alloy systems and ternary systems with a dilute solution of the third component: For a given alloy and a given set of process parameters the microstructure with the lowest undercooling, or else with the highest growth temperature is assumed to be selected by the system. Modeling then requires the ability to calculate the growth temperature of all possible competing morphologies: single phase cells and dendrites, planar and cellular eutectics but also two-phase eutectic dendrite-like fingers. Fukumoto and Kurz [134] presented phase and microstructure selection maps for solidification of Fe–Cr–Ni alloys with about 18 wt.% Cr, calculated with interface response functions for plane and dendritic front as well as eutectic and banded growth structures. The maps were calculated for two different temperature gradients as being representative for unidirectional solidification and solidification after laser remelting, analyzed experimentally. Resonable agreement between experimental and calculated microstructure selection maps was reported.

Today, fundamental knowledge about the operating point of more complex two-phase morphological structures, e.g. eutectic cells and dendrites (fingers) in ternary and multicomponent alloys is in the early stage of development (see Section 4.1). Himemiya et al. [110,135,136] were the first to attempt at deriving approximate analytical solutions for growth of competing morphologies in a ternary eutectic alloy system, based on the classification and strategy proposed by McCartney et al. [97]. The growth model for two-phase eutectic cells and dendrites with rod-like intracellular eutectic structure [135] is based on the assumption that the undercooling can be expressed as a sum of the eutectic undercooling and the constitutional undercooling of the cellular tip. The first is calculated in analogy to the Jackson–Hunt theory assuming that the eutectic spacing is much smaller then the tip radius of the cell or dendrite. The constitutional undercooling of the needle-like cellular tip is estimated by applying the extremum condition or the array stability criterion following the analysis of Burden and Hunt [137] or Hunt and Lu [138] for binary alloys, formulated with respect to the third component as long as the overall alloy composition lies on the univariant groove. For alloys outside the groove the expression proposed by McCartney at al. for ternary single phase dendrites is used [97]. Reality is much more complex but despite of the many assumptions used, Himemiya's model can be a guide for experiment design, whenever rod-like eutectics are concerned.

4.3. The solidification path and microstructure formation

Driven by industrial demand, extensive research is dedicated to microstructure evolution during solidification of multicomponent, multiphase alloys. It mainly focuses on the impact of microse-

gregation associated to the solidification of the primary phase on the subsequently forming phases and solidification defects. The main differences to the issues discussed in Section 4.1 stem from the fact that all stages of solidification are transient and inherently unstable. Moreover solidification rates are typically high, such that departure from thermodynamic equilibrium is considerable. Along the solidification path, element partition between solid and liquid obeys rather the Scheil–Gulliver approximation [139,140], that assumes no diffusion in the solid and complete mixing in the liquid. For most multicomponent alloys this means, that several secondary and tertiary phases will form in the terminal stage of solidification, some of them being possibly metastable. Consecutive steps of phase formation are indeed pertinent to many technologically important alloys, here we give just few examples:

For Nb-bearing Ni- and Fe-base superalloys, minor variations of alloy composition affect the type and amount of phases formed in interdendritic regions. Laves phases and Nb-carbides NbC are known to form in eutectic reactions. The systematic study by DuPont et al. [141–143], spanning from DTA-experiments and microsegregation analysis of fusion welded samples to modeling microsegregation and phase formation along the solidification path of various alloys, highlights the major role played by carbon.

In heat and corrosion resistant steels, typically rich in chromium and molybdenum the formation of metastable M_7C_3-carbides during solidification were shown to enhance the precipitation of the brittle sigma phase during annealing [144]. In a Cr- and Mo-rich Co-base alloy used to manufacture surgical implants by investment casting Ramiréz et al. [3] reported that the sigma phase formed in the terminal stage of solidification.

In aluminum alloys the formation of intermetallic phases, rich in Fe, Mn and Si, received much attention not only because of the complexity related to the selection of stable or metastable phases [145], but also due the fact that some of them increase the propensity for defect formation [146].

Modeling microsegregation and the formation of secondary phases, while taking into account solid state, or back diffusion and kinetic effects related to dendrite tip undercooling and dendrite arm coarsening proved to be effective. Since the first analytical model of Mehrabian and Flemings [147] for a ternary alloy many numerical models of microsegregation have been developed and reviewed by Kraft and Chang [35]. The models usually employ a 1D approximation of the dendrite arm geometry as plate, cylinder or sphere and solve the multicomponent diffusion equations coupled to a solidification model and to thermodynamic data. For details on model formulations for multi-component, multiphase alloys the reader is guided to Kraft et al [148], Chen et al. [149] and Boettinger et al. [150] for closed systems and to Doré et al. [151] and Cefalu et al. [152] who extended the microsegregation models for closed systems to open systems, thus allowing for coupling to macrosegregation models.

The comparison between model predictions and experimental data is quite troublesome, mainly due to the fact that microsegregation or else element distribution profiles measured via microprobe line scans do not necessarily pass through the center-line of a dendrite arm. To overcome this problem, area scan methods have been proposed by Flemings et al. [153] and Gungor [154]: They are based on the idea, that the concentrations of the individual components, measured at each point of the scan area obey a specific mutual relationship that is cartelistic (and unequivocal) for each moment of the solidification history. Once an appropriate expression Ψ for this mutual relationship is found, e.g. the difference between the concentrations of two individual components, it is straight forward to arrange Ψ in ascending order and to apply probability statistics as to relate Ψ to a value $p \in [0, 1]$ representing the fraction solid. This transformation of ‘‘composition versus position’’ plots to ‘‘composition versus fraction solid’’ plots is very much convenient for comparison between model predictions and

experimental data. As to account for the 3D nature of experimental microstructures, this analysis is much enhanced, when the data used stem from large area scans or from area scans in several metallographic sections.

Lacaze and Lesoult [155] applied the method to assess microsegregation in directionally solidified Al-alloys. Xie et al. [156] used it for comparing experimentally observed microsegregation profiles and phase fractions to model predictions for ternary Al–Cu–Mg alloys. Based on their work Liang et al. [157] discussed the importance of reliable thermodynamic data, and proceeded to re-evaluate the ternary phase diagram as to improve the quality of the model predictions. Recently, Xie et al. [158] presented an investigation of microstructure and microsegregation in the aluminum alloy 7050 containing 11 components, that forms six different intermetallic phases in subsequent eutectic reactions during solidification. Modeling was based on a modified Scheil model taking into account solid state diffusion, dendrite undercooling and coarsening, with dynamic coupling to phase diagram calculations. Fig. 19, reproduced by courtesy of Xie et al. [158], shows a comparison between calculated and measured microsegregation for one of the components of the alloy and calculated phase fractions. The measurements stem from area scans over large sections from within a directionally solidified sample, processed under a thermal gradient $G = 4.5 \times 10^3$ K/m with a cooling rate of 0.45 K/s. From Fig. 19a, representing the distribution of Mg as function of the fraction of solid, it is obvious that a pure Scheil calculation would overestimate both, segregation and the total amount of eutectic phases. Fig. 19b shows the calculated fractions for each of the intermetallic phases as function of temperature. A good agreement between calculated and experimentally measured microsegregation and phase fractions was reported.

For the future one may expect phase field simulations to contribute to this topic as well. First results of computing microsegregation during dendritic solidification of a five component Ni-base superalloy and comparing the computed results with line scan measurements of microsegregation in unidirectionally solidified samples are due to Warnken et al. [162]. It may be expected further that phase field simulations prove effective to handle microstructures, where different phases solidify at different locations in space, a situation where application of one-dimensional microsegregation models is inadequate. Linking microstructure simulations based on phase field models to macroscopic solidification modeling may be regarded as a long-term task.

The most prominent advantage of microsegregation and microstructure models formulated for open systems is, that they can be efficiently integrated into macroscopic solidification models. For reasons of computational efficiency it may be necessary to adopt simplifications, yet this is a way to

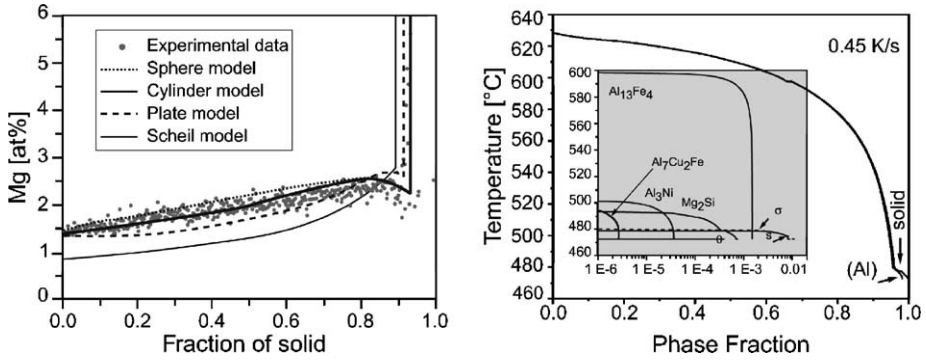

Fig. 19. Calculated and measured distribution of Mg (a) and model-calculated phase fractions as a function of temperature (b) for the aluminum alloy 7050 after directional solidification in a temperature gradient of 4.5×10^3 K/m with a cooling rate of 0.45 K/s reprinted by courtesy of Xie et al. [158].

couple local microstructure evolution to mass, momentum and energy transport at the scale of a casting. Schneider et al. [159] were the first to calculate macrosegregation in a multicomponent steel while including the full effects of buoyancy driven fluid flow for single phase solidification. Krane et al. [160] developed a macroscopic model for the solidification of ternary alloys including multiple phase formation during terminal solidification and applied it to simulate convective phenomena during solidification of Pb–Sb–Sn alloys [161].

5. Modeling microstructure evolution

Solidification, like every first order phase transition, leads to the formation of dissipative structures throughout the stages of nucleation and growth. The morphological features of the emerging solid phases are dependent on the growth kinetics, e.g. on the dissipation of heat and solute generated at the solid/liquid interface(s) under the conditions imposed by the solidification process. The solid/liquid interface(s) are moving free boundaries, that adjust their local curvature in order to enhance dissipation under the constraints imposed by interfacial energy. Modeling microstructure evolution then requires the solution of partial differential equations that describe transport in terms of heat and solute diffusion without making a priori assumptions on the shape of the solid/liquid interface(s) e.g. on their location in space and time. In his recent paper Sekerka [163] gives a beautiful overview on the evolution of models for crystal growth morphology, spanning from sharp interface models with shape preserving solutions to phase field models that emerged during the 1980s based on the Cahn–Hilliard and Ginzburg–Landau field theoretic approaches.

Phase field models emerged to be the method of choice for complex microstructure evolution problems and accordingly a vast variety of models have been proposed. The reader is directed to the recent reviews by Ode et al. [164], Chen [165] and Boettinger et al. [166]. Here we only briefly describe the main concept of phase field models and proceed with presenting some applications of phase field models to multiphase growth in binary and multicomponent alloys.

5.1. The phase field concept

The phase field concept is based on defining a non-conserved structural order parameter ϕ (the phase field), which maps the phase state of the system as a function of space and time.

The order parameter is assigned the value $\phi = 1$ in the bulk solid phase and $\phi = 0$ in the bulk liquid phase. It changes smoothly between these limits over a thin transition layer that defines the diffuse interface as an equivalent of the classical sharp interface. This structural order parameter is often interpreted as the local volume fraction of the given solid phase, or as the amplitude of the dominant Fourier component of the singlet density in the solid.

One then expands the free energy density or the entropy density of the inhomogeneous system (liquid + solid phases) with respect to the non-conserved order parameter and other conserved parameters, retaining only the spatial derivatives allowed by symmetry considerations.

In a very general form, when several order parameters ϕ_i are needed for different individual phases and multicomponent alloys with several solute species (c_k) are considered the free energy of the system can be described as a local functional of these fields:

$$F = \int \mathrm{d}V \left\{ \sum_{i,j} a_{ij}(\nabla\phi_i \nabla\phi_j) + \sum_{k,l} b_{kl}(\nabla c_k \nabla c_l) + \cdots + f(\{\phi_i\}, \{c_k\}, T, \ldots) \right\} \tag{14}$$

The terms that contain the field gradients account for the interfacial energies. The coefficients a_{ij} and b_{kl} may depend on temperature, orientation, and the field variables. The function $f(\{\phi_i\}, \{c_k\}, T)$ represents the free energy density as function of the phase mixture, the phase composition and temperature and a double well potential in the interface region.

Following the phenomenology of non-equilibrium statistical mechanics, and relying on the principle of positive entropy production or decreasing free energy, partial differential equations are derived for the evolution of the phase field and other field variables like concentration or temperature. The equation of motion differs for non-conserved fields (such as the structural order parameter, orientation, magnetization, etc. whose spatial integral may vary with time) and conserved fields (whose spatial integral is constant, e.g., chemical composition) read:

Non-conserved dynamics:

$$\dot{\phi}_i = -M_{\phi_i} \frac{\delta F}{\delta \phi_i} + \zeta_i \tag{15}$$

Conserved dynamics:

$$\dot{c}_i = \nabla \left\{ M_{c_i} \nabla \frac{\delta F}{\delta c_i} \right\} + \zeta_j \tag{16}$$

Here M_i are the appropriate field mobilities related to the driving force for the interfaces, while ζ_i are Gaussian white noises (random current for conserved quantities) with an amplitude determined by the fluctuation dissipation theorem Elder et al. [167], Karma and Rappel [168]; Pavlik and Sekerka [169,170]. The evolution of the non-conserved phase variables ϕ_i is thus coupled to those of the conserved fields Hohenberg and Halperin [171]. These equations of motion are usually highly non-linear, and together with the appropriate Langevin-noise, they are able to describe complex solidification morphologies.

While attempts have been made to derive the free energy functional of solid–liquid systems on physical grounds Oxtoby [172,173], the molecular theories are often too complicated to address complex solidification problems. Therefore, in most approaches phenomenological free energy or entropy functionals are used, whose form owes much to the Ginzburg–Landau models used in describing magnetic phase transitions.

The central task is indeed the construction of the free energy functional. In this regard the present phase field models can be divided into two groups, according to the specific target they aim at: The first group aims at gaining basic physical insight into the solidification process, and accordingly, the free energy functional is constructed on the basis of the typical features/symmetries of the phase diagrams Karma and Rappel [168], Elder et al. [167]; Drolet et al. [174]. The second group aims more at engineering applications for all possible phase diagrams and hence the free energy functional is chosen so that basic properties of the diffuse interface are recovered while combined with detailed alloy thermodynamics. The main issue here is the ability to treat multiphase transitions in multicomponent alloys. In Section 5.3 these models are described in more detail.

5.2. *Phase field modeling applied to multiphase solidification in binary alloys*

Phase field models for multiphase solidification problems like growth of eutectics, peritectics and monotectics in binary alloys have been developed by several groups.

Eutectics: Following the first two-phase-field model of eutectics by Wheeler et al. [175], Nestler and Wheeler [176] used a similar model to investigate lamellar spacing selection including the annihilation of lamellae, tip splitting and various instabilities during eutectic solidification in a model

binary system in 2D. As done earlier by Karma [177], they recovered the Jackson and Hunt scaling for lamellar spacing and undercooling versus growth velocity. On the basis of 2D simulations, Regel et al. [178] found that freezing rate oscillations lead to refined eutectic microstructures. Akamatsu et al. [86] have shown that when relaxing Cahn's assumption that lamellar growth is locally normal to the interface, lamellar eutectic growth may be stable for a wide range of spacings. A three-phase-field model has been used by Folch and Plapp [179] to simulate oscillatory limit cycles in 2D lamellar growth showing that a continuous transition from small amplitude oscillations to successive invasions with varied lamellar spacings can occur. Recent qualitative simulations of fibrous eutectic growth were performed in 3D by Apel et al. [180] based on a three-phase-field model showing splitting instability. Recently Kim et al. [181] published a eutectic phase field model for isotropic and anisotropic interface energies and kinetic coefficients and used the isotropic model for 2D computations of lamellar eutectic growth patterns in the binary eutectic CBr_4–C_2Cl_6 system for the eutectic and a hypereutectic alloy composition. They quantitatively compare the computed transitions from basic lamellar patterns to oscillatory and tilted patterns and the characteristic scales of the patterns with the experimental results reported by Ginibre et al. [85]. Transition between rod and lamellar structures as a function of the volume fraction of the minor phase, and spacing selection via rod-branching has been observed in recent 3D multiphase-field simulations for a binary system by Lewis et al. [182]. Phase field theory of nucleation and equiaxed growth in binary eutectics will be addressed in Section 6.2.

Peritectics: Peritectic solidification in a binary Fe–C alloy has been investigated in 2D by Tiaden et al. [183] and Tiaden and Grafe [184] showing δ-ferrite dendrites being enveloped by austenite as the peritectic reaction proceeds. Lee et al. [185] found that the growth of the gamma phase follows parabolic growth kinetics in 1D isothermal transformations and linear kinetics in 1D continuous cooling. Nestler and Wheeler [176] qualitatively reproduced various peritectic morphologies, including the development of properitectic phase particles. Transition from bands to island growth in directional peritectic solidification has been studied in 2D, using a two-phase-field model by Lo et al. [70], which includes the nucleation of the peritectic phase. The simulations have born out remarkable similarity to experimental patterns [83].

Monotectics: Nestler et al. [186] developed a single-phase-field and a two-phase-field model of monotectic solidification, which incorporates coupling to hydrodynamics and temperature-dependent interfacial free energies, hence the Marangoni convection. They presented 2D simulations of lamellar monotectic structures, that exhibit wetting phenomena, coarsening, and particle pushing, and show a striking similarity to experimental patterns.

5.3. Phase field models for multiphase solidification in multicomponent alloys

The extension of multiphase-field models from binary to multicomponent alloys is rather new: Plapp and Karma [187] formulated a eutectic phase field model for a binary eutectic with a dilute ternary impurity and simulated the formation of eutectic colonies in 2D. They reported a good agreement with their earlier stability analysis [72] regarding the destabilization of the initially planar lamellar front due to long-wavelength modes. They observed furthermore, that Cahn's hypothesis of lamellae growing perpendicular to the envelope of the solidification front, is violated. A striking similarity to 2D experiments [104] has been achieved.

More general phase field models for multicomponent alloys rely on a direct coupling of the phase field equations to thermodynamic databases and equilibrium calculations. Qin et al. [188] proposed a direct linking to thermodynamic calculations for a two-phase field model. Kobayashi et al. [189] proposed a two-phase field model for ternary alloys including the thermodynamic data via an a priori

calculated tie-line map of the ternary phase diagram. Chen et al. [190] reported on direct linking the Ti-base thermodynamic database from CompuTherm and the kinetic software DICTRA to a two-phase field model for modeling growth of precipitates in the ternary system Ti–Al–V. Cha et al. [191] reported on coupling thermodynamic data to a two-phase field model. The only model that presently applies to multiphase transformations in multicomponent alloys is based on the multiphase-field model, initially developed by Steinbach et al. [192] and Steinbach and Pezolla [193] for unary alloys. Tiaden et al. [183] extended to it to binary alloys and Grafe et al. [194] and Böttger et al. [195] to multicomponent alloys. In the following we present the coupling of the phase field equations to thermodynamic calculations according to Böttger et al. [195].

In the n-phase field system, the following set of equations describe the evolution of the individual phase fields, based on a double obstacle formulation:

$$\dot{\phi}_i = \sum_{j \neq i} \mu \left\{ \sigma \left[(\phi_j \nabla^2 \phi_i - \phi_i \nabla^2 \phi_j) + \frac{\pi^2}{2\eta^2}(\phi_i - \phi_j) \right] + \frac{\pi}{\eta} \sqrt{\phi_i \phi_j} \Delta G_{ij} \right\} \tag{17}$$

The last term in the equations accounts for the thermodynamic driving force. ΔG_{ij} [J/cm^3] is the free energy difference between two interacting, multicomponent phases i and j. This term links the evolution of the phase fields to that of the composition fields.

In the multi-phase regions the model explicitly calculates the phase compositions c_i^k, which are linked to the mixture composition:

$$c^k = \sum_{i=1}^{N} \phi_i c_i^k \tag{18}$$

Diffusion is treated by making use of the volume averaging method and taking into account off-diagonal diffusion terms:

$$\dot{c}^k = \nabla \sum_{i=1}^{N} \phi_i j_i^k = \nabla \sum_{i=1}^{N} \phi_i \sum_{l=1}^{n-1} D_i^{kl} \nabla c_i^l \tag{19}$$

Coupling the phase field model to thermodynamic databases and calculations is performed via the TQ interface developed by Thermo-Calc AB and the Thermo-Calc software. It provides three types of information:

a) the relation between the compositions c_i^k and c_j^k of the phases i and j in contact;
b) the thermodynamic driving force ΔG_{ij} for Eq. (17);
c) some conditions for nucleation of secondary phases.

For diffusion-controlled processes a quasi-equilibrium approach is applied. The quasi-equilibrium is defined by construction of parallel tangent planes to the Gibbs energy functions f_i and f_j and expressed in Eq. (20). The driving force ΔG_{ij} results from small deviation from local equilibrium.

$$a^k = \frac{\mathrm{d}f_i}{\mathrm{d}c_i^k} = \frac{\mathrm{d}f_j}{\mathrm{d}c_j^k} \tag{20}$$

The driving force is then expressed as:

$$\Delta G_{ij} = f_i - f_j + \sum_{k=1}^{n-1} a^k (c_i^k - c_j^k) \tag{21}$$

Inside the diffuse interface the mass balance applies, giving the additional condition:

$$c^k = \sum_i \phi_i c_i^k \tag{22}$$

Eqs. (20)–(22), can be solved to get the quasi-equilibrium phase compositions c_i^k and c_i^k and the driving force ΔG_{ij}. This is done in a pair-wise manner for all phase interactions ij. Together with a thermodynamic database that gives the Gibbs free energy functions f_i and f_j even complex multi-component and multiphase problems can be solved in this way.

Tremendous calculation times would be needed to perform the thermodynamic calculations in each time step and for all interface grid points. Therefore, together with the equilibrium calculation the slopes p_{ij}^k and q_{ji}^k of the liquidus and the solidus plane in the directions of every component k =1, 2, 3, …, N are extracted at the equilibrium compositions c_i^k and c_j^k, respectively. This procedure corresponds to a local linearization of the phase diagram for each interface cell in the calculation domain. The local linearization is sufficient for most cases and thermodynamic calculations has to be done only from time to time, when the local compositions or the temperature changed considerably compared to their values at the previous thermodynamic calculation step.

The local linearization procedure yields the following expressions for the evolution of the temperature, the compositions and the driving force for the time interval in between successive thermodynamic calculations. For sake of clarity, the values obtained from the last thermodynamic calculation are indexed with an upper zero.

$$T_{ij} = T_{ij}^0 + \sum_k^{N-1} p_{ij}^k (c_i^k - c_{ij}^k) \tag{23}$$

from the liquidus plane or

$$T_{ij} = T_{ij}^0 + \sum_k^{N-1} q_{ij}^k (c_i^k - c_{ij}^k) \tag{24}$$

from the solidus plane

The driving force ΔG_{ij} can be derived, if T is the actual temperature at this grid point:

$$\Delta G_{ij} = -\Delta S_{ij}^{\text{trans}} (T - T_{ij}) + \Delta G_{ij}^0 \tag{25}$$

Using Eqs. (23)–(25) the extrapolated local phase compositions can finally be calculated, taking into account all phases "l" that coexist with phases i and j, e.g. in triple points.

$$c_i^k = \frac{c^k - \sum_{l=1}^M \phi_l (c_{li}^{0,k} - c_{il}^{0,k} m_{li}^k / m_{il}^k)}{\sum_{l=1}^M \phi_l m_{li}^k / m_{il}^k} \tag{26}$$

$$c_j^k = \frac{c^k - \sum_{l=1}^M \phi_l (c_{lj}^{0,k} - c_{jl}^{0,k} m_{lj}^k / m_{jl}^k)}{\sum_{l=1}^M \phi_l m_{lj}^k / m_{jl}^k} \tag{27}$$

This model proves efficient for handling arbitrary multicomponent alloys for which thermodynamic databases are available. The local linearization procedure helps to reduce computational time significantly, but needs special care for alloy systems with stoichiometric phases or with complex

equilibrium surfaces that change the sign of the slope relative to one of the components (re-entrant surfaces).

5.4. Phase field modeling applied to multiphase solidification in multicomponent alloys

With the above presented model Böttger et al. [195–197] simulated the evolution of the microstructure during unidirectional solidification of superalloys using the thermodynamic database "NiFe-Data" from Thermotech Ltd. Warnken et al. [162] discussed simulation results performed by using the Ni–Al–Cr–Ta–W database developed by N. Dupin in comparison with experimental data, with focus on microsegregation patterns obtained by microprobe measurements in the unidirectionally solidified five-component model alloy Ni–Al 5.8 wt.%–Cr 8.98 wt.%–Ta 7.94 wt.%–W 8.84 wt.%.

Böttger et al. [198] used the above described model coupled to the thermodynamic database "TCFe" from Thermo-Calc AB to simulate dendritic growth of δ-ferrite and the peritectic reaction and subsequent transformation to austenite in the ternary alloy Fe–C 1 at.%–Mn 1 at.% for directional solidification in a temperature gradient of $G = 20 \times 10^3$ K/m and a cooling rate of 1 K/s. The diffusion coefficient of the two components C and Mn were assumed to be equal in the liquid phase $D_l^{\mathrm{C}} = D_l^{\mathrm{Mn}} = 2 \times 10^{-9}$ m^2/s but different in the solid phases $D_{\mathrm{s}}^{\mathrm{C}} = 5.2 \times 10^{-10}$ m^2/s and $D_{\mathrm{s}}^{\mathrm{Mn}} = 1.2 \times 10^{-11}$ m^2/s, respectively. A snapshot in Fig. 20 shows the quicker homogenization of carbon inside the austenitic layer compared to manganese.

Application of the model to nonvariant eutectic growth of the ternary alloy Al–Cu 13.07 at.%–Ag 16.97 at.% was reported by Apel et al. [113]. No direct coupling to the thermodynamic database was done, since at the nonvariant eutectic point the phase diagram can be easily linearized. Since in 2D, the stacking sequence can be considered a free parameter, once isotropic and equal interfacial energies are assumed for all interfaces in the system (here 10^{-5} J/cm^2), the question emerged, how different stacking sequences would affect the pattern and the undercooling of the eutectic interface. Computa-

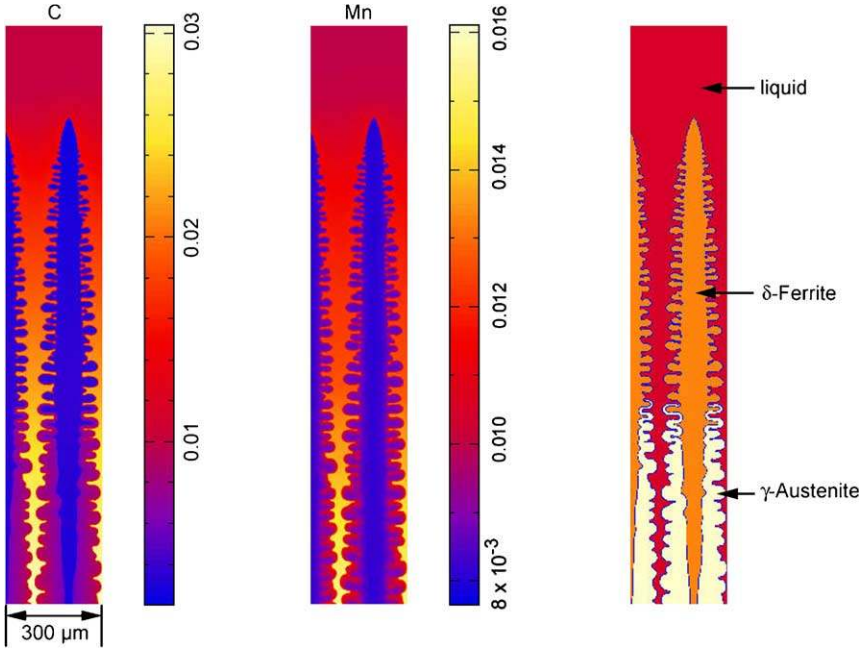

Fig. 20. Solidification of Fe–C 1 at.%–Mn 1 at.% at a cooling rate of 1 K/s in a temperature gradient of 20×10^3 K/m. Shown are the composition maps of carbon and manganese in atom fractions as well as the phase map.

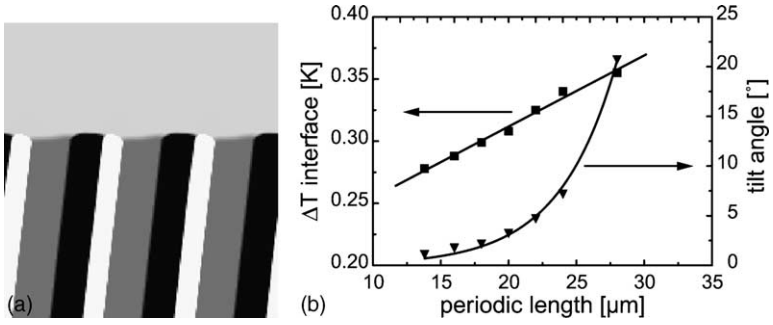

Fig. 21. Snapshot of the eutectic interface growing with the stacking sequence ABC and a periodic length (spacing) of 15 μm in tilted mode. The phases are identified form the Ag-composition map: A = Ag_2Al (white), B = α(Al) (grey) and C = Al_2Cu (black) (a). The average interface undercooling and the tilt angle increase both with increasing periodic length (b).

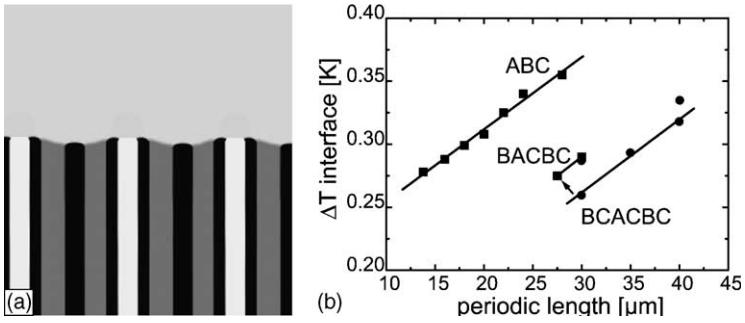

Fig. 22. Snapshot of the eutectic interface growing with the mirror symmetric stacking sequence BCACBC and a periodic length (spacing) of 30 μm in axisymmetric growth (a). The phases are identified form the Ag-composition map: A = Ag_2Al (white), B = α(Al) (grey) and C = Al_2Cu (black). The average interface undercooling decreases with decreasing periodic length, being lower than that of the simple ABC stacking sequence for the same periodic length (b).

tions for different stacking sequences, including ABC, BACBC, BCACBC were performed with the diffusion coefficients in the liquid assumed to be 10^{-9} m^2/s for all components and the kinetic coefficient $\mu = 5 \times 10^{-4}$ $cm^4/J\,s$ for all interfaces. All simulations were made for directional solidification conditions in a temperature gradient of 5×10^3 K/m with a pulling velocity of 1×10^{-6} m/s. It was found that the ABC sequence is tilted with respect to the growth direction. In contrast to tilted modes in binary alloys the tilted growth is a direct consequence of the lack of mirror symmetry in ABC sequence. Fig. 21a shows a snapshot of the eutectic interface for the ABC stacking and Fig. 21b the tilt angle and the interface undercooling for different lamellar spacings, represented by the periodic length. Higher order, mirror symmetric sequences accomplished axisymmetric growth and were shown to lower the interface undercooling for equal periodic lengths, as summarized in Fig. 22a and b.

6. Nucleation

In previous sections, we have discussed microstructure evolution during growth-controlled processes, relevant to steady-state growth occurring in unidirectional solidification, i.e. when the

effect of nucleation and the transients associated with early stages of growth have faded away. In other cases, microstructure strongly depends on the nucleation of the primary and the subsequently forming phases. With the exceptions of extremely pure samples or small liquid droplets, where homogeneous nucleation may occur, solidification of undercooled liquids starts with heterogeneous nucleation of the primary phase, followed by a heterogeneous nucleation of subsequent phases, processes that may be initiated by pre-existing crystalline phases that act as heterogeneous nucleation sites.

Nucleation is a complex fluctuation phenomenon. Atomistic simulations performed by Swope and Andersen [199] and ten Wolde and Frenkel [200] show that even during homogeneous crystal nucleation in a single component liquid, several local atomic arrangements (bcc, fcc, hcp, icosahedral) compete, of which often a metastable phase wins. For binary and multicomponent alloys the complexity increases, as the composition of nuclei enters as an extra state variable.

In the following we give a short introduction to nucleation theory with an emphasis on recent developments concerning multicomponent nucleation. First recent extensions of the classical theory are covered, then we proceed by reviewing field-theoretic models for homogeneous and heterogeneous nucleation in binary and multicomponent systems. Finally, a brief discussion of experimental methods relevant to nucleation problems is presented.

6.1. The kinetic theory of nucleation

The classical (kinetic) theory of nucleation had been formulated by Farkas [201] and Becker and Döring [202], and was adopted for first-order phase transformations in condense matter by Turnbull and Fisher [203]. This approach relies on a set of master equations that consider only single molecule attachment and detachment processes (a good approximation at the early stages of solidification). Analytical and numerical treatments of the problem indicate that, after a transient period, steady state conditions are established, under which the nucleation rate, e.g. the net volumetric formation rate of critical fluctuations can be expressed as:

$$J = J_0 \exp\left\{\frac{-W^*}{kT}\right\}, \tag{28}$$

where J_0 is the nucleation prefactor, W^* the free energy of critical fluctuations, while k and T are Boltzmann factor and temperature.

In determining the free energy of the heterophase fluctuations, the classical nucleation theory relies on the droplet model (introduced by Gibbs for studying phase stability) that views the heterophase fluctuations as spherical crystals, whose free energy is expressed in terms of their radius R, the volumetric Gibbs free energy difference Δg (<0) between the bulk crystal and the undercooled liquid, and the interface free energy γ:

$$W = \left(\frac{4\pi}{3}\right) R^3 \Delta g + 4\pi R^2 \gamma \tag{29}$$

yielding a maximum of $W^* = (16\pi/3)\gamma^3/\Delta g^2$ at the critical radius $R^* = -2\gamma/\Delta g$.

The adaptation of the classical droplet model to heterogeneous nucleation has been reviewed by Christian [204]. The spherical cap model accounts for the free energy reduction due to the creation of a triple junction line between the nucleating solid, the liquid, and a preexisting solid phase (container wall, foreign particle, primary phase) that acts as a substrate. Under such conditions only a fraction of the homogeneous nucleus needs to be formed by random fluctuations, a phenomenon that reduces the height of the nucleation barrier. For a planar interface, the critical fluctuation is a spherical cap, whose size is determined by the contact angle θ between the solid–substrate and liquid–solid interfaces,

which in turn is fully determined by the free energies of the solid–liquid, solid–substrate and liquid substrate interfaces. Under such conditions, the ratio of the free energies of the heterogeneous and homogeneous nuclei is given by the catalytic potency factor:

$$f(\theta) = \tfrac{1}{4}(2 + \cos\theta)(1 - \cos)^2 \tag{30}$$

The drawbacks of the classical nucleation theory emerge from those of the droplet model, which relies on the thermodynamic properties the macroscopic bulk phase, when calculating the free energy of near critical clusters. According to the experiments by Howe [205] and Huisman et al. [206] and computer simulations, as reviewed by Laird and Haymet [207], the crystal–liquid and crystal–glass interfaces are diffuse on the molecular scale, extending over several molecular layers, the interface thickness being comparable to the size of critical fluctuations and the interface region reaches their centers. This invalidates the main assumption of the droplet model, that the interface thickness is negligible with respect to the size of the fluctuations. Two main issues then emerge:

a) Derivation of a kinetic theory that incorporates the differences in the diffusion of the individual species.
b) Derivation of cluster models that include the dependency of the Gibbs free energy and interface free energy on the cluster composition and size for multicomponent alloys.

Since recent reviews by Gunton [208], Gránásy and James [209], and Oxtoby [172] covered part of the new developments, here we cover only theories that address nucleation in binary and multicomponent alloys.

The classical kinetic model has been extended to nucleation in binary and multi-component systems by several authors: Kozisek and Demo [210], Wilemski and Wyslouzil [211], Slezov et al. [212], Kozisek et al. [213], Slezov and Schmelzer [214] and Schmelzer et al. [215]. A general theory, which includes coagulation/splitting has been worked out for phase separation by Binder and Stauffer [216]. An essential finding is that for significantly different diffusivities of the constituents, the nucleation pathway may avoid the saddle point of the free energy surface as shown by Greer et al. [217]. Recent work by Kelton [218] takes into account the coupled fluxes of interfacial attachment and long-range diffusion. Numerical solution of the model shows that the time-dependent nucleation rate scales with the smaller mobility, and that the steady-state rates and induction times differ significantly from values predicted by the classical theory. The kinetics of formation of phases with arbitrary stoichiometric compositions in multicomponent solid solutions has been addressed by Slezov and Schmelzer [214]. A new theoretic approach for nucleation and growth in multicomponent systems has very recently been proposed by Schmelzer et al. [215] which relies on an improved cluster model that considers non-bulk local states. Improved cluster models have been put forward by several authors for binary systems: Taking into account the finite interface thickness, the phenomenological diffuse interface theory by Gránásy [219] removed the several orders of magnitude difference seen between theory and experiment for vapour condensation [220] and crystal nucleation [221]. This model has been generalized by Volkman et al. [222] and Moire and Herlach [223] for nucleation in ternary alloys and by Kvamme [224] for multicomponent alloys. In a recent model of *binary* nucleation, Schmelzer [225] determines the optimum composition of nuclei via minimizing the sharp-interface cluster free energy with respect to cluster composition, while relying on a composition dependent interface free energy and regular solution thermodynamics, an approach that, much like the field theoretic models, leads to diminishing nucleation barrier approaching the spinodal. A multicomponent version of the theory has been presented recently [215]. While the application of the model for condensation and phase separation has been developed in details, its generalization for crystallization in liquids and

glasses is less straightforward, as it requires the knowledge of the interfacial free energy as a function of temperature and composition. This needs further theoretical considerations/atomistic modeling.

Recent developments of the theory for heterogeneous nucleation include the analysis of the role played by impurities and adsorbed layers published by Cantor [226] and Greer [227], and a refined description of the kinetics which controls the mechanisms of phase selection in solidification of atomized droplets by Perepezko [228].

6.2. Field-theoretic models for homogeneous and heterogeneous nucleation

The nanometer sized heterophase fluctuations, that form on typical experimental time scales, can be naturally handled in the framework of continuum or field theoretic models that are able to address local states, which differ from the bulk crystal or liquid states. In the field theoretic models, the local physical state is characterized by locally averaged (coarse grained) order parameters. The free energy of the inhomogeneous system is then a functional of order parameter field. Similarly to the case of the classical droplet model, where the critical fluctuation represents a maximum of the free energy function, here the critical fluctuation is an extremum of the free energy *functional*.

In the past decades various field theoretic models have been worked out for crystal nucleation. Many of them are direct descendants of the single-order-parameter gradient theories by van der Waals [229] and Cahn and Hilliard [230]. In the classical field theories of crystallization the free energy of the inhomogeneous system (liquid + critical fluctuation) is approximated by local *functionals* of the type:

$$F = \int \mathrm{d}r^3 \{f[m(\boldsymbol{r})] + \kappa(\nabla m)^2\} \tag{31}$$

where m is a structural order parameter, that can be viewed as the amplitude of the dominant Fourier component of the crystal singlet density, κ is a constant, while the free energy density f has a double-well form asymmetric in the undercooled state. The square-gradient term of the order parameter yields a diffuse interface. The critical fluctuation (nucleus) is a saddle point of the free energy functional. The respective $m(\boldsymbol{r})$ emerges as a non-trivial solution of the Euler–Lagrange equation,

$$\frac{\delta F}{\delta m} = \frac{\partial f}{\partial m} - 2\kappa\nabla^2 m = 0 \tag{32}$$

under boundary conditions $m \to m_0$ for $|\boldsymbol{r}| \to \infty$ and $\nabla m \to 0$ for $|\boldsymbol{r}| \to 0$, where $\delta F/\delta m$ is the functional derivative of the free energy with respect to the order parameter field, while $m_0 = 0$ is the order parameter of the undercooled liquid.

Assuming spherical symmetry, a reasonable approximation considering the weak anisotropy of the interface free energy, the Euler–Lagrange equation reduces to an ordinary differential equation. If the free energy density is of piecewise parabolic form, the Euler–Lagrange equation is linearized, and the solution can be found analytically. This method has been used to address such problems as crystal nucleation and growth in one-component liquids by Bagdassarian and Oxtoby [231] and Gránásy and Oxtoby [232], hard-sphere crystallization by Wild and Harrowell [233] and crystallization in the presence of metastable phases by Gránásy and Oxtoby [66]. A more complex single-order-parameter Cahn–Hilliard model relying on a quadratic free energy density has been recently used by Gránásy et al. [234] to evaluate interfacial properties from nucleation experiments.

An extension of the Cahn–Hilliard theory to nucleation in multicomponent phase separating systems is due to Hoyt [67]. Other important generalizations of the Cahn–Hilliard theory are the Hohenberg–Halperin [171] C-type field theoretic models in which the time evolution of the non-conserved structural order parameter is coupled to other fields of conserved dynamics.

Probably the most important continuum model that is able to address simultaneous crystal nucleation and growth is the phase field theory. The proper statistical mechanical treatment of the nucleation process requires the introduction of uncorrelated Langevin-noises into the governing equations with amplitudes that are determined by the fluctuation-dissipation theorem as shown by Pavlik and Sekerka [169,170]. Such an approach has been used to describe eutectic solidification in a binary model system by Elder et al. [167] and Drolet et al. [174]. A similar technique has been applied by Gránásy et al. [235] for simulating the nucleation of primary dendritic particles with different crystallographic orientations. To describe differences in the crystallographic orientation, following Kobayasi et al. [236,237], they introduced a non-conserved orientational field. However, they extended this orientational field to the liquid, where it fluctuates in time and space, a feature reflecting the short-range order of the liquid. The large-scale simulations performed using this model are depicted in Fig. 23. The simulations permitted the determination of the Kolmogorov-exponent that describes the time evolution of the crystalline fraction for multigrain dendritic solidification and for anisotropically growing particles interacting via diffusion fields ('soft impingement'). The results are consistent with devitrification experiments performed on metallic glasses. Pusztai and Gránásy [182] have extended this approach to the nucleation and growth of eutectic phases during equiaxed solidification. Fig. 24 shows the simulated multigrain structures obtained for the freezing of hypo-eutectic, eutectic, and hyper-eutectic Ag–Cu melts.

Besides simulating the nucleation process, the phase field theory can be used to calculate the height of the nucleation barrier as reported by Roy et al. [238] and Gránásy et al. [235]. Fixing the model parameters such that the free energy and thickness of the equilibrium planar interface is recovered, good quantitative agreement has been achieved with computer simulations for the

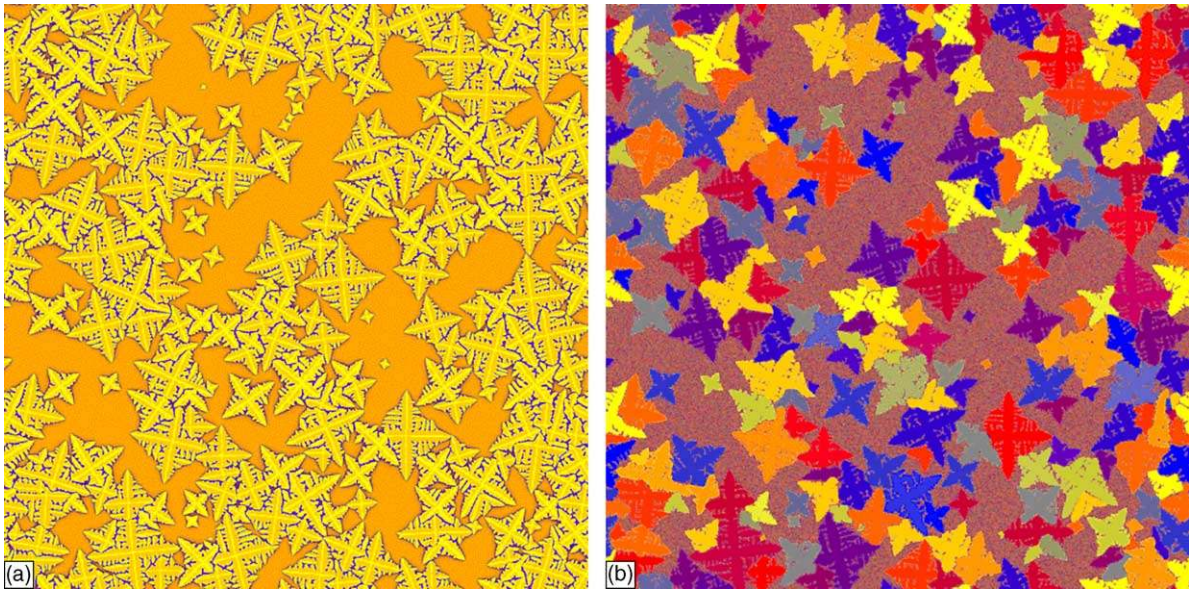

Fig. 23. 2D dendritic solidification of a binary Ni–Cu alloy as predicted by the phase field theory at 1574 K and a supersaturation of 0.8. By the end of solidification about 300 dendritic particles form. The calculation has been performed on a 3000 × 3000 grid. In (a) the color map represents compositions, with yellow and blue corresponding to the solidus and liquidus compositions, respectively, while the intermediate compositions are shown by colors that interpolate linearly between these two. In (b) the colors denote crystallographic orientations: When the fast growth direction is upward, 30, or 60° left, the grains are colored blue, yellow, or red, respectively, while the intermediate angles are denoted by a continuous transition among these colors. Owing to the four-fold symmetry, orientations that differ by 90° multiples are equivalent.

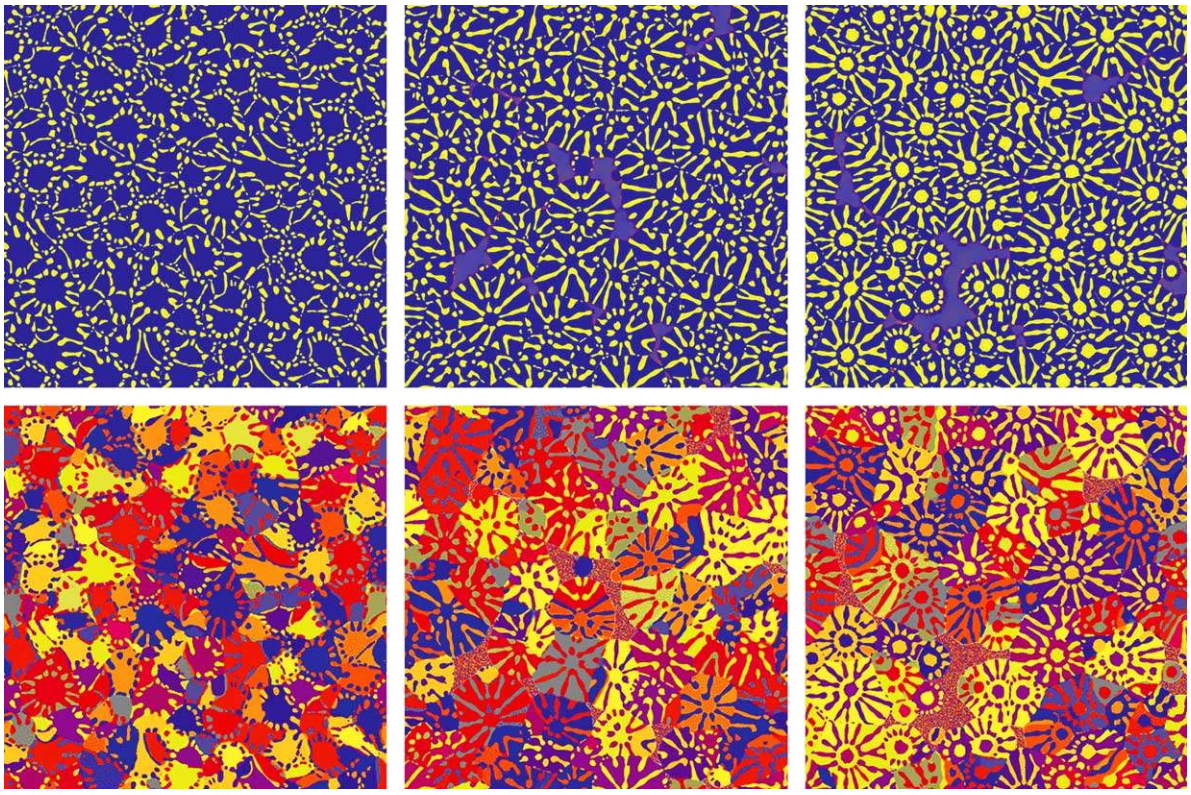

Fig. 24. Equiaxed solidification in hypo-eutectic (c_{Cu} = 0.3), eutectic (c_{Cu} = 0.35), and hyper-eutectic (c_{Cu} = 0.4) Ag–Cu liquids at 900 K as simulated by the phase field model. Composition maps are shown in the top row, the respective orientation maps are in the bottom row. The simulations were performed in 2D on a 1000 × 1000 grid. In the composition maps, continuous change from blue to yellow indicates compositions varying from c_{Cu} = 0 to 1, respectively. In the orientation maps, different colours stand for different crystallographic orientations in the laboratory frame.

Lennard–Jones system, and with experiments on ice nucleation in undercooled water [235]. Similar results have been obtained for crystal nucleation in the hard-sphere system Gránásy et al. [239]. For binary Ni–Cu alloys reasonable values have been obtained [235] for the temperature and composition dependence of the interface free energy, which yields reasonable critical undercoolings for electromagnetically levitated droplets.

Extension of the phase field approach to nucleation in multicomponent alloys is possible by the introduction of further composition fields, which increases the number of coupled Euler–Lagrange equations that define the critical fluctuation. It appears, that the most efficient tools of our theoretical inventory for describing crystal nucleation are such continuum models. Further improvement in the accuracy of the phase field theory might be expected, if the intuitively chosen functions for defining the free energy density are replaced by others, derived on physical grounds. Advances have been recently made in this direction by Gránásy and Pusztai [240].

A few remarks on handling nucleation in phase field simulations: As mentioned above, the natural way to handle nucleation in simulations is the addition of Langevin-noise terms to the governing equations. Nonetheless, modeling of nucleation via Langevin-noise is often prohibitively time consuming. One remedy is simply to increase the amplitude of the noise. This, however, raises the possibility that the fluctuations, which initiate solidification, will most likely significantly differ from the real critical fluctuations. To avoid practical difficulties associated with modeling noise-

induced nucleation, crystallization in simulations is often initiated by randomly placing supercritical particles into the simulation window (e.g., Simmons [241]). An alternative method has been proposed by Gránásy et al. [235], who first calculate the properties of the critical fluctuations and then place such critical fluctuations randomly into the simulation window, while also adding Langevin-noise that decides whether these nuclei grow or dissolve.

Solidification in the presence of walls is of great practical importance. In casting, solidification usually starts by heterogeneous crystal nucleation on the walls of the mould. With the exception of extremely pure samples, even volume nucleation happens mostly via a heterogeneous mechanism on the surface of floating foreign particles, as suggested by Turnbull [242]. Particulate additives are widely used as grain refiners, to reduce grain size by enhancing the nucleation rate. Nonetheless, heterogeneous nucleation is probably the only stage of solidification where the micromechanism of the process is largely unknown. While the phase field method has been used to address problems that incorporate heterogeneous nucleation, this process is usually mimicked by introducing supercritical particles into the simulation window. Such a procedure has been adopted by Lo et al. [70] and [83] for the simulation of island versus coupled growth in binary peritectic alloys.

The effect of foreign particles on growth morphology has been modeled by introducing orientation pinning centers (areas of constant but random orientation) into the phase field theory by Gránásy et al. [243]. The model has successfully been applied for describing the formation of disordered dendritic structures ('dizzy' dendrites) observed in clay filled polymer blend films.

Recently, steps have been made towards a physical modeling of heterogeneous nucleation within the phase field theory. Castro [244] introduced walls into a single-order-parameter theory (one-component case) by assuming a no-flux boundary condition at the interface ($n\nabla\phi = 0$, where n is the normal vector of the wall), which results in a contact angle of 90° at the wall–solid–liquid triple junction. Langevin-noise is then introduced to model nucleation. Following a similar route, Gránásy et al. [245] introduced chemically inert surfaces ($\boldsymbol{n}\nabla\phi = 0$ and $\boldsymbol{n}\nabla c = 0$ at the wall perimeter) into a binary phase field theory while incorporating an orientation field, and performed simulations to address heterogeneous nucleation on foreign particles, rough surfaces and in confined space (porous matter and channels). Fig. 25 depicts the evolution of the microstructure in a freezing binary liquid throughout the stages of heterogeneous nucleation at rough surfaces and growth.

6.3. Nucleation in transient stages of unidirectional solidification

At the beginning of Section 6 we noted that nucleation can be ignored for steady state stages of growth. For transient stages however, nucleation is an important issue even for directional solidification processes, especially for multiphase alloys. Such transient regimes occur after initiating the multiphase directional growth from a solid seed or when sudden or continuous changes of the process parameters take place, such as velocity jumps or accelerated/decelerated velocity profiles. Furthermore, oscillatory growth can occur in special cases of eutectic, peritectic or monotectic solidification as a result of periodic switching between competing morphologies. In all these cases nucleation is effectively at work.

From recent studies of the initial transient in a transparent binary, slightly off-eutectic alloy CBr_4–C_2Cl_6 Akamatsu [86] reported two different mechanisms of initiation of coupled eutectic growth: In the first case the second solid phase forms via multiple nucleation events at the bottom of cellular grooves present at the initially single-phase solid/liquid interface of the primary phase. This mechanism leads to a very small grained eutectic structure. In the other case the second phase emerges

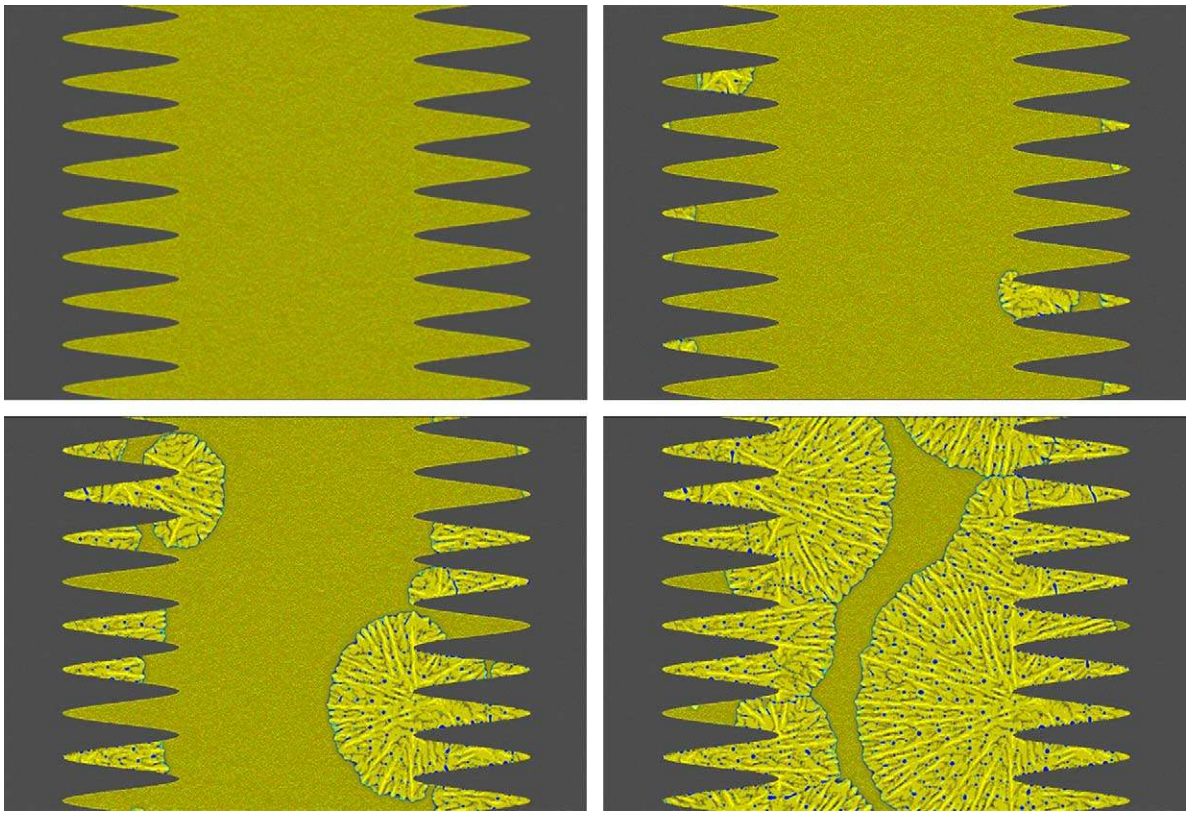

Fig. 25. Heterogeneous crystal nucleation on rough (sinusoidal) surfaces in a binary liquid as predicted by the phase field simulations. Composition maps are shown (liquidus—blue, solidus—yellow, gray—walls). Note the preference for nucleation inside the 'notches' of the wall.

via some migration process e.g. along liquid grain boundaries, at a few points of the interface shortly after the onset of the primary phase growth. It then spreads across the solid/liquid interface of the primary phase in form of a thin oscillatory structure usually called ''surface dendrite''. Coupled growth is initiated through the growth of the primary phase between the branches of the surface dendrite. This mechanism, called invasion, is not stopped, though significantly slacken down, when the solid/liquid interface of the primary phase exhibits a cellular structure. It usually leads to a large eutectic grain size.

For ternary alloys the initiation of coupled growth is likewise related to nucleation. But nucleation may be significant also with regard to the steady state growth of eutectic cells that exhibit lamellae or rod termination at the intracellular boundaries. Presently it is still unclear how the intracellular eutectic structure resolves lamellae or rod multiplication to compensate for termination.

Ruggiero and Rutter [109] discussed possible mechanisms of lamellae multiplication, i.e. spacing reduction, for three-phase non-variant eutectic growth, as to explain the double binary structure observed in the Bi-BiIn-γ(Sn) eutectic: The authors argued with Smith [246], that it is topologically impossible for a lamellar three-phase eutectic with an ABCABC stacking sequence to branch while maintaining the stacking sequence. Branching, as the single mechanism of spacing reduction can only occur for rod-like eutectics in 3D. For all other situations, nucleation is at play. This is an important issue for all 2D simulations or experiments in very thin (quasi 2D) cells. In 3D or bulk samples spacing adjustment may operate quite differently.

Based on experiments and simulations of peritectic growth in binary Ni–Cr alloys Lo et al. [70,83] pointed out the importance of nucleation for island growth and the oscillations between islands and coupled growth.

Hecht et al. [247] presented unidirectional solidification experiments in the hypoeutectic ternary alloy Al–Mn 1 wt.%–Si 3 wt.%, where deliberately added TiB_2-particles acted as heterogeneous nucleation sites for the $Al_{15}Mn_3Si_2$-phase. Instead of achieving coupled irregular eutectic growth between α(Al) and $Al_{15}Mn_3Si_2$, the $Al_{15}Mn_3Si_2$-phase nucleated as individual particles ahead of the solid/liquid interface of α(Al) and was subjected to pushing. During pushing the $Al_{15}Mn_3Si_2$-particles continued growing, while the exchange of solute species between α(Al) and $Al_{15}Mn_3Si_2$ in eutectic reaction occurred across the liquid gap established in the pushing configuration.

On the experimental side the detailed analysis of nucleation events during transient growth stages is not easy, especially for metallic alloys where direct observation of the solid/liquid interface is not straight forward: From several real time and in situ techniques that have been developed for detecting the solid/liquid interface in metallic alloys [248–251] one alone is able to measure not only the position but also the temperature of the advancing interface and thus nucleation undercooling in bulk samples: This method was developed by Salvi [252] and Garandet [253] and is based on the measurement of the Seebeck voltage and electrical resistance of the solidifying sample with reference to a sample that contains a non-moving solid/liquid interface. All these techniques are rather new. Their application to growth transients and to nucleation and early growth problems will hopefully be consolidated in future.

7. Conclusions and perspectives

Research of microstructure formation during multiphase solidification in multicomponent alloys attracts steadily increasing interest, as well-established thermodynamic databases are now available for many alloy systems. Two main focal points may be identified: First, fundamental research focuses mainly on the morphological stability and the dynamic behavior of multiphase patterns during steady state growth in unidirectional solidification. Secondly, widespread interest is directed towards multiphase microstructures, evolving in successive steps of phase formation along the solidification path of multicomponent alloys, during casting, welding and brazing. Naturally, these two areas differ in the strategies, the experimental techniques and computational tools employed. However, both of them depend on the availability of reliable data for thermodynamic, diffusion kinetic, and interfacial properties. While thermodynamic databases and the related computational thermodynamic tools are fairly advanced for many multicomponent alloy systems, diffusion kinetic and interface property data are scarce. However, progress is expected due to ongoing research in several groups.

The most challenging questions regarding the formation and the dynamic behavior of multiphase patterns in coupled growth refer to the interplay between the small-scale pattern and the larger scale morphologies. Anisotropy, of both topological and crystalline origin, seems to play an important role. The use of comparative 2D/3D experimental strategies, as well as the application of in situ observation techniques for transparent organic analogues and metallic alloys are expected to deepen our future understanding. Selected aspects will benefit from experiments performed under microgravity conditions, whenever buoyancy induced fluid flow needs to be supressed.

As far as the multiphase microstructures evolving in successive steps of phase formation along the solidification path of multicomponent alloys are concerned, much progress has been made in the past years via coupling solidification models to thermodynamic calculations and reliable databases. Further advances in the field of multi-scale modeling are expected from developing models that

account for phase volume effects, such that fluid flow from volume contraction and porosity formation become tractable.

In the past decade the phase field model emerged as an efficient method for describing multiphase microstructures evolving during solidification of multicomponent alloys. Application to alloys of practical interest is feasible, by coupling to thermodynamic databases. Further progress is expected from developing and applying improved computational methods (e.g., Amberg [254]) that will facilitate 2D and 3D simulations with realistic technical parameters. Incorporation of fluid flow and stress/strain will allow the treatment of volume changes during phase transitions. New models may also contribute to the advance of the field. A remarkable new field theoretic approach by Elder et al. [255] allows for atomistic modeling of the solid–liquid transition on diffusive time scales, while naturally incorporating crystal anisotropy, elastic and plastic deformations, grain boundaries, cracks, epitaxy, etc. (Elder and Grant [256]). The model has recently been generalized for eutectic solidification and dendritic growth (Elder [257]). With the ever-increasing power of computers, this approach may take over many of the tasks of the phase field theory.

Nucleation remains perhaps the least understood stage of solidification, not in terms of its basic physics on the atomistic or molecular scale, but mainly because it is rarely addressed as an integral part of solidification problems. Phase field simulations that include Langevin-noise to model thermal fluctuations and an extra field describing crystallographic orientation, emerged as a powerful tool for handling nucleation and growth. At present such simulations are limited to multiphase solidification of binary alloys in 2D. Their application to coupled growth may shed light to the initiation of coupled growth and the spacing adjustment mechanisms. In this respect, phases that select specific mutual orientations appear as the most challenging cases. Future extension to ternary alloys could open the route for addressing such complex problems as lamellae multiplication in eutectic cells, driven by the need to compensate for lamellae termination at intracellular boundaries.

Summarizing, one may say that the key to success for achieving a level of understanding similar to the one established for binary alloys also for multicomponent, multiphase alloys is the close interaction between experimental and modeling activities linking thermodynamic, and thermophysical properties to microstructure evolution. This interactive approach, termed knowledge based materials engineering, is expected to render the design of multiphase materials more prolific and their production and quality easier to control.

Acknowledgement

The paper is based on discussions within the frame of the topical team ‘‘Solidification in multicomponent, multiphase systems’’. The topical team was established by the European space agency ESA and supported in the period 2000–2002, as to join industrial and academic experience for defining clear-cut topics that benefit from investigations under reduced gravity. We wish to thank our industrial partners, G.U. Grün from Hydro-Aluminium, Germany, Ch. Sigli from Pechiney, France, H.A. Kuhn from Wieland Werke AG, Germany and A. Howe from Corus, U. Kingdom for many fruitful discussions. We also wish to thank O. Minster and D.J. Jarvis from ESA for their continuous support. Finally, we wish to thank B. Sundman from Thermo-Calc AB, Sweden for sharing with us his vast experience in the field of computational thermodynamics. Special thanks are due to H. Bramann from the Foundry Institute of the RWTH Aachen, Germany, for supplying Fig. 1b and to Y.A. Chang and F. Xie from the University of Wisconsin-Madison, USA, for courteously supplying Fig. 19a and b.

References

[1] J.N. DuPont, J.R. Michael, B.D. Newbury, Welding J. 78 (1999) 408.
[2] M.J. Perricone, J.N. DuPont, M.J. Cieslak, Met. Mater. Trans. 34A (2003) 1127.
[3] L.E. Ramiréz, M. Castro, M. Méndez, J. Lacaze, M. Herrera, G. Lesoult, Scripta Mater. 47 (2002) 811.
[4] W. Khalifa, F.H. Samuel, J.E. Gruzleski, Met. Mater. Trans. 34A (2003) 807.
[5] G. Sauthoff, Intermetallics 8 (2000) 1101.
[6] A. Sayir, S.C. Framer, Acta Mater. 48 (2000) 4691.
[7] V.M. Orera, J.I. Peña, R.I. Merino, J.A. Lázaro, J.A. Vallés, M.A. Rebolledo, Appl. Phys. Lett. 71 (1997) 2746.
[8] A. Larrea, L. Contreras, R.I. Merino, J. Llorca, V.M. Orera, J. Mater. Res. 15 (2000) 1314.
[9] L. Kaufman, H. Bernstein, Computer Calculation of Phase Diagrams with Specific Reference to Refractory Materials, Academic Press, New York, 1970.
[10] N. Saunders, A.P. Miodownik, CALHAD, Elsevier Science, New York, 1998.
[11] A.T. Dinsdale, Calphad 15 (1991) 317.
[12] SGTE (Scientific Group Thermodata Europe), Solution Database of January 1994.
[13] M. Hillert, L.I. Staffanson, Acta Chem. Scand. 24 (1970) 3618.
[14] B. Sundman, J. Ågren, J. Phys. Chem. Solids 42 (1981) 297.
[15] Y.M. Muggianu, M. Cambino, J.P. Bros, J. Chim. Phys. 22 (1975) 83.
[16] O. Kubaschewski, C.B. Alcock, P.J. Spencer, Materials Thermochemistry, sixth ed. Pergamon Press, Oxford, 1993.
[17] V.T. Witusiewicz, U. Hecht, S. Rex, F. Sommer, J. Alloy. Compd. 337 (2002) 189.
[18] H. Flandorfer, E. Hayer, J. Alloy. Compd. 296 (2000) 112.
[19] M. Asta, V. Ozolins, C. Woodward, JOM 53 (2001) 16.
[20] S.G. Fries, B. Sundman, Phys. Rev. B 66 (2002) 012203.
[21] G. Gosh, A. van de Walle, M. Asta, G.B. Olson, Calphad 26 (2002) 491.
[22] F. Lechermann, Ph.D. Thesis, Max Planck Institut für Metallforschung, Stuttgart, 2003.
[23] B. Sundman, B. Jansson, J.O. Anderson, Calphad 9 (1985) 153.
[24] G. Eriksson, K. Hack, Metall. Trans. 21 (1990) 13.
[25] Pandat — Software for multicomponent phase diagram calculation, Computherm LLC, 437S., Yellowstone Drive, Suite 217, Madison, Wi 53719, USA.
[26] R.H. Davis, A.T. Dinsdale, T.G. Chart, T.I. Barry, M. Rand, High Temp. Sci. 26 (1990) 251.
[27] H.L. Lukas, J. Weiss, E.-T. Hening, Calphad 6 (1982) 229.
[28] U.R. Kattner, W.J. Boettinger, S.R. Corriell, Z. Metallkd. 87 (1996) 522.
[29] U.R. Kattner, JOM 49 (1997) 14.
[30] J. Ågren, F.H. Hayes, L. Hoglund, U.R. Kattner, B. Legendre, R. Schmid-Fetzer, Z. Metallkd. 93 (2002) 128.
[31] V.T. Witusiewicz, U.Hecht, S. Rex, J. Alloys Comp., submitted for publication.
[32] Raj K., Dictra (Diffusion controlled transformations) — Software developed within the project COSMOS (Computer supported modeling of steel transformations) funded by Volkswagenstiftung and Land Nordrhein-Westfalen, 1988–1993.
[33] J. Ågren, J. Phys. Chem. Solids 43 (1982) 421.
[34] J.O. Andersson, J.J. Ågren, J. Appl. Phys. 72 (1992) 1350.
[35] G. Inden, Calphad and Alloy Thermodynamics, TMS Annual Meeting, Seattle, WA, TMS, Warrendale, PA, 17–21 February 2002, p. 108.
[36] T. Kraft, Y.A. Chang, JOM 49 (1997) 20.
[37] P. Kopczyński, W.J. Rappel, A. Karma, Phys. Rev. Lett. 77 (1996) 3387.
[38] S.J. Langer, in: Proceedings of the Les Houches Summer School, Session XLVI, Elsevier, New York, 1987.
[39] E. Ben Jacob, P. Garik, Nature 343 (1990) 523.
[40] L. Onsager, Phys. Rev. 37 (1931) 405.
[41] J.S. Kirkaldy, D.J. Young, Diffusion in the Condensed State, Insitute of Metals, London, 1987.
[42] W.B. Brockman, J.E. Morral, Profiler: Diffusion Couple Software to Predict Concentration Profiles and [D] (available from J.-E. Morral, Department of Metallurgy and Institute of Materials Sciene, University of Connecticut).
[43] T.H. Cohen, M.E. Glicksman, Model. Simul. Mater. Sci. Eng. 3 (1995) 585.
[44] C.E. Campbell, W.J. Boettinger, T. Hansen, P. Merewether, B.A. Mueller, Third International Alloy Conference, Estoril, Portugal, 30 June–5 July 2002, submitted for publication.
[45] C.E. Campbell, W.J. Boettinger, U.R. Kattner, Acta Mater. 50 (2002) 775.
[46] D.G. Miller, Acta Mater. 46 (7) (1998) 5993.

[47] J.P. Praisey, Int. J. Heat Mass Transfer 32 (1989) 2385.
[48] G. Frohberg, H. Kraatz, H. Wever, A. Lodding, H. Odelius, Defect Diff. Forum 66–69 (1989) 295.
[49] J.P. Garandet, G. Mathiak, V. Botton, P. Lehman, A. Griesche, Int. J. Thermophys. 25 (2004) 249.
[50] V. Botton, P. Lehmann, R. Bolcato, R. Moreau, R. Haettel, Int. J. Heat Mass Transfer 44 (2001) 3345.
[51] D.P. Woodruff, The Solid-Liquid Interface, Cambridge University Press, 1973.
[52] N. Eustathopoulos, Int. Met. Rev. 28 (1983) 189.
[53] K.F. Kelton, Solid State Phys. 45 (1991) 75.
[54] C. Vahlas, N. Eustathopoulos, D. Camel, J. Cryst. Growth 92 (1988) 253.
[55] M. Gündüz, J.D. Hunt, Acta Metall. 33 (1985) 1651.
[56] N. Maraşli, J.D. Hunt, Acta Mater. 44 (1996) 1085.
[57] P.W. Voorhees, S.R. Coriell, G.B. McFadden, J. Cryst. Growth 67 (1984) 425.
[58] R.E. Napolitano, et al. in: B.K. Dhindaw (Ed.), International Conference on Solidification Science and Processing, Science Publisher Inc., Bangalore, 2001, p. 73.
[59] J.J. Hoyt, M. Asta, A. Karma, Mater. Sci. Eng. 41 (2003) R121.
[60] R. Sigub-Aga, B.B. Laird, Phys. Rev. B 66 (2002) 4106.
[61] R.L. Davidchak, B.B. Laird, Mol. Phys. 97 (1999) 833.
[62] B.J. Kooi, Acta. Mater. 51 (2003) 4653.
[63] S.A. Dreggia, P. Wynblatt, Acta Metall. Mater. 39 (1991) 771.
[64] D.B. Zhang, G. Rao, P. Wynblatt, Modelling Simul. Mater. Sci. Eng. 1 (1993) 639.
[65] Y.C. Shen, D.W. Oxtoby, Phys. Rev. Lett. 77 (1996) 3585.
[66] L. Gránásy, D.W. Oxtoby, J. Chem. Phys. 112 (2000) 2410.
[67] J.J. Hoyt, Acta Metall. Mater. 38 (1990) 1405.
[68] C. Huang, M. Olvera de la Cruz, P.W. Vorhees, Acta Mater. 47 (1999) 4449.
[69] A.A. Wheeler, W.J. Boettinger, G.B. McFadden, Phys. Rev. E (1993) 1893.
[70] T.S. Lo, A. Karma, M. Plapp, Phys. Rev. E 63 (2001) 031504.
[71] R. Roth, S. Dietrich, Phys. Rev. E 62 (2000) 6926.
[72] M. Plapp, A. Karma, Phys. Rev. E 60 (1999) 6865.
[73] K.A. Jackson, J.D. Hunt, Trans. Metall. Soc. AIME 236 (1966) 1129.
[74] W. Kurz, P.R. Sahm, Gerichtet erstarrte eutektische Werkstoffe, Springer, Berlin, 1975.
[75] R. Trivedi, J.T. Mason, J.D. Verhoeven, W. Kurz, Metall. Trans. 22 (1991) 252.
[76] J. Hunt, S.Z. Lu, Crystallisation of eutectics, monotectis and peritectics, in: D. Hurle (Ed.), Handbook of Crystal growth, vol. 2b, Elsevier, Amsterdam, 1994, p. 1111 ff.
[77] R. Grugel, A. Hellawell, Metall. Trans. A 12A (1981) 669.
[78] A. Kamino, S. Kumai, H. Tezuka, Mater. Sci. Eng. A 146 (1991) 105.
[79] B. Mujamdar, K. Chattopadhyay, Metall. Trans. A 27A (1995) 2053.
[80] S.R. Coriell, W.F. Mitchell, B.T. Murray, J.B. Andrews, Y. Arikawa, J. Cryst. Growth 179 (1997) 647.
[81] C. Stöcker, L. Ratke, J. Cryst. Growth 212 (2000) 324.
[82] M. Vandyoussefi, H.W. Kerr, W. Kurz, Acta Mater. 48 (2000) 2297.
[83] T.S. Lo, S. Dobler, M. Plapp, A. Karma, W. Kurz, Acta Mater. 51 (2003) 599.
[84] A. Karma, A. Sarkissian, Metall. Mater. Trans. 27A (1996) 635.
[85] M. Ginibre, S. Akamatsu, G. Faivre, Phys. Rev. E 56 (1997) 780.
[86] S. Akamatsu, M. Plapp, G. Faivre, A. Karma, Phys. Rev. E 66 (2002) 30501.
[87] C. Misbah, K. Kassner, R. Baumann, Phys. Rev. E 48 (1995) R2751.
[88] C. Misbah, K. Kassner, A. Valance, D. Temkin, Phys. Rev. E 48 (1993) 91.
[89] M. Durand-Charre, F. Durand, J. Cryst. Growth 13–14 (1972) 747.
[90] P.J. Fehrenbach, H.W. Kerr, P. Niessen, J. Cryst. Growth 16 (1972) 209.
[91] P.R. Sahm, M. Lorenz, J. Mater. Sci. 7 (1972) 793.
[92] G. Garmong, Metall. Trans. 2 (1971) 2025.
[93] D.J.S. Cooksey, A. Hellawell, J. Inst. Met. 95 (1967) 183.
[94] F. Mollard, B. Lux, J.C. Hubert, Z. Metallkd. 65 (1974) 461.
[95] M.D. Rinaldi, R.M. Sharp, M.C. Flemings, Metall. Trans. 3 (1972) 3139.
[96] H.A. Quac Bao, F.C.L. Durand, J. Cryst. Growth 15 (1972) 291.
[97] D.G. McCartney, J.D. Hunt, R.M. Jordan, Metall. Trans. A 11 (1980) 1243.
[98] D.G. McCartney, R.M. Jordan, J.D. Hunt, Metall. Trans. A 11 (1980) 1251.
[99] J. De Wilde, L. Froyen, S. Rex, Scripta Mater., submittet for publication.

[100] I. Yamauchi, S. Ueyama, I. Ohnaka, Mater. Sci. Eng. A208 (1996) 101.
[101] S.V. Raj, I.E. Locci, Intermetallics 9 (2001) 217.
[102] U. Hecht, V.T. Witusiewicz, A. Drevermann, S. Rex, Adv. Eng. Mater., submitted for publication.
[103] V. Datye, J.S. Langer, Phys. Rev. B 24 (1981) 4155.
[104] S. Akamatsu, G. Faivre, Phys. Rev. E 61 (2000) 3757.
[105] L.R. Morris, W.C. Winegard, J. Cryst. Growth 5 (1969) 361.
[106] H.W. Kerr, A. Plumtree, W.C. Winegard, J. Inst. Metals 93 (1964) 63.
[107] J.D. Holder, B.F. Oliver, Meter. Trans. 5 (1974) 2423.
[108] C.T. Rios, S. Milenkovic, S. Gama, R. Caram, J. Cryst. Growth 237–239 (2002) 90.
[109] M.A. Ruggiero, J.W. Rutter, Mater. Sci. Technol. 11 (1995) 136.
[110] T. Himemiya, T. Umeda, Mater. Trans. JIM 40 (1999) 665.
[111] V.T. Witusiewicz, L. Sturz, U.Hecht, S. Rex, Acta Mater., submitted for publication.
[112] L. Sturz, V.T. Witusiewicz, U.Hecht, S. Rex, J. Cryst. Growth, submitted for puiblication.
[113] M. Apel, B. Böttger, V. Witusiewicz, U. Hecht, I. Steinbach, Adv. Eng. Mater., submitted for puiblication.
[114] H. Sens, N. Eustathopoulos, D. Camel, J.J. Favier, Acta Metall. Mater. 40 (7) (1992) 1783.
[115] T. Buchholz, Master's thesis, Universität zu Köln, 1994.
[116] J.J. Favier, J. De Goer, Results of Spacelab-15th European Symposium Material Sciences Under Microgravity, SP 222, ESTEC Noordwijk, 1984, p. 127.
[117] F.D. Lemkey, R.W. Hertzberg, J.A. Ford, Trans. Metall. Soc. AIME 233 (1966) 334.
[118] P. Bárczy, J. Sólyom, Mater. Sci. Forum 77 (1991) 113.
[119] G. Müller, P. Kyr, Results of Spacelab-1, 5th European Symposium Material Sciences Under Microgravity, SP 222, ESTEC Noordwijk, 1984, p. 141.
[120] B. Drevet, D. Camel, M. Dupouy, J.J. Favier, Acta Mater. 44 (10) (1996) 4071.
[121] S. Steinbach, Ph.D. thesis RWTH Aachen, 2004, in preparation.
[122] D. Ma, W.Q. Jie, Y. Li, S.C. Ng, Acta Mater. 46 (1998) 3203.
[123] P. Magnin, R. Trivedi, Acta Metall. Mater. 39 (1991) 453.
[124] K.B. Kim, J. Liu, N. Maraşli, D.J. Hunt, Acta Metall. Mater. 43–46 (1995) 2143.
[125] S.R. Coriell, G.B. McFadden, W.F. Mitchell, B.T. Murray, J.B. Andrews, Y. Arikawa, J. Cryst. Growth 224 (2001) 145.
[126] L. Ratke, Metall. Mater. Trans, 34A (2003) 449.
[127] C. Stöcker, L. Ratke, J. Cryst. Growth 203 (1999) 582.
[128] R.N. Grugel, A. Hellawell, Metall. Trans. A 15 (1984) 1626.
[129] B. Vinet, C. Potard, J. Cryst. Growth 61 (1983) 355.
[130] J.B. Andrews, A. Sandlin, R. Merrick, Adv. Space Res. 11 (1991) 291.
[131] B. Dhindaw, D. Stefanescu, A. Singh, P. Curreri, Metall. Trans. 19A (1988) 2839.
[132] W.J. Boettinger, S.R. Coriell, A.L. Greer, A. Karma, W. Kurz, M. Rappaz, R. Trivedi, Acta Mater. 48 (2000) 43.
[133] P. Gilgien, W. Kurz, Mater. Sci. Eng. A 178 (1994) 199.
[134] S. Fukumoto, W. Kurz, ISIJ Int. 39 (1999) 1270.
[135] T. Himemiya, Mater. Trans. JIM 40 (1999) 675.
[136] T. Himemiya, Mater. Trans. JIM 40 (2000) 437.
[137] M.H. Burden, J.D. Hunt, J. Cryst. Growth 22 (1974) 99.
[138] J.D. Hunt, S.-Z. Lu, Metall. Trans. 27A (1996) 611.
[139] E. Scheil, Z. Metallkd. 34 (1941) 70.
[140] G.M. Gulliver, J. Inst. Met. 9 (1913) 120.
[141] J.N. DuPont, C.V. Robino, J.R. Michael, M.R. Notis, A.R. Marder, Met. Mater. Trans. 29A (1998) 2785.
[142] J.N. DuPont, C.V. Robino, A.R. Marder, M.R. Notis, Met. Mater. Trans. 29A (1998) 2797.
[143] J.N. DuPont, C.V. Robino, A.R. Marder, Acta Mater. 46 (13) (1998) 4781.
[144] G.R. Garcés, J. Le Coze, J.L. Garin, R.L. Mannheim, Scripta Mater. 50 (2004) 651.
[145] C.M. Allen, K.A.Q. O'Reilly, B. Cantor, P.V. Evans, Prog. Mater. Sci. 43 (1998) 89.
[146] N. Roy, A.M. Samuel, F.H. Samuel, Met. Mater. Trans. 27A (1996) 415.
[147] R. Mehrabian, M.C. Flemings, Metall. Trans. 1 (1970) 455.
[148] T. Kraft, M. Rettenmayr, H.E. Exner, Modell. Simul. Mater. Sci. Eng. 4 (1996) 161.
[149] S.L. Chen, Y.A. Chang, Metall. Trans. A 23 (1992) 1038.
[150] W.J. Boettinger, U.R. Kattner, D.K. Banerjee, in: B.G. Thomas, C. Beckermann (Eds.), Modeling of Casting, Welding and Advanced Solidification Processes VIII, The Minerals, Metals & Materials Society, Warendale, 1998, p. 159.

[151] X. Doré, H. Combeau, M. Rappaz, Acta Mater. 48 (2000) 3951.
[152] S.A. Cefalu, M.J.M. Krane, Mater. Sci. Eng. A359 (2003) 91.
[153] M.C. Flemings, D.R. Poirier, R.V. Barone, H.D. Brody, J. Iron Steel Inst. 208 (1970) 371.
[154] M.N. Gungor, Metall. Trans. 20A (1989) 2529.
[155] J. Lacaze, G. Lesoult, ISIG Int. 35 (1995) 658.
[156] F.-Y. Xie, T. Kraft, Y. Zuo, C.-H. Moon, Y.A. Chang, Acta Mater. 47 (2) (1999) 489.
[157] H. Liang, T. Kraft, Y.A. Chang, Mater. Sci. Eng. A292 (2000) 96.
[158] F. Xie, X. Yan, L. Ding, F. Zhang, S. Chen, M.G. Chu, Y.A. Chang, Mater. Sci. Eng. A355 (2003) 144.
[159] M.C. Schneider, C. Beckermann, Met. Mater. Trans. 26 (1995) 2373.
[160] M.J.M. Krane, F.P. Incropera, Int. J. Heat Mass Transfer 40 (16) (1997) 3827.
[161] M.J.M. Krane, F.P. Incropera, Int. J. Heat Mass Transfer 40 (16) (1997) 3837.
[162] N. Warnken, B. Böttger, D. Ma, V. Vitusevych, U. Hecht, S. G. Fries, N. Dupin, in: J. Lecomte-Beckers, et al. (Eds.), Materials for Advanced Power Engineering, part I, Liege, Belgium, Forschungszentrum Jülich, Jülich, 29 September–2 October 2002, p. 315.
[163] R.F. Sekerka, J. Cryst. Growth, in press.
[164] M. Ode, S.G. Kim, T. Suzuki, ISIJ Int. 41 (2001) 1076.
[165] L.Q. Chen, Annu. Rev. Mater. Res. 32 (2002) 113.
[166] W.J. Boettiger, J.A. Warren, C. Beckermann, A. Karma, Annu. Rev. Mater. Res. 32 (2002) 163.
[167] K.R. Elder, F. Drolet, J.M. Kosterlitz, M. Grant, Phys. Rev. Lett. 72 (1994) 677.
[168] A. Karma, W.-J. Rappel, Phys. Rev. E 60 (1999) 3614.
[169] S.G. Pavlik, R.F. Sekerka, Physica A 268 (1999) 283.
[170] S.G. Pavlik, R.F. Sekerka, Physica A 277 (2000) 415.
[171] P.C. Hohenberg, B.I. Halperin, Rev. Mod. Phys. 49 (1977) 435.
[172] D.W. Oxtoby, Liquids, Freezing and Glass Transition, Elsevier, Amsterdam, 1991.
[173] D.W. Oxtoby, Annu. Rev. Mater. Res. 32 (2002) 39.
[174] F. Drolet, K.R. Elder, M. Grant, J.M. Kosterlitz, Phys. Rev. E 61 (2000) 6705.
[175] A.A. Wheeler, G.B. McFadden, W.J. Boettinger, Proc. R. Soc. Lond. A 452 (1996) 495.
[176] B. Nestler, A.A. Wheeler, Physica D 138 (2000) 114.
[177] A. Karma, Phys. Rev. E 49 (1994) 2245.
[178] L.L. Regel, W.R. Wilcox, D. Popov, F. Li, Acta Astronaut. 48 (2001) 101.
[179] R. Folch, M. Plapp, in: B. Nestler, H. Emmerich (Eds.), Proceedings of the International Workshop on Computational Physics, Springer, Dresden, 2002, in press.
[180] M. Apel, B. Böttger, H.J. Diepers, I. Steinbach, J. Cryst. Growth 237 (2002) 154.
[181] S.G. Kim, W.T. Kim, T. Suzuki, M. Ode, J. Cryst. Growth 261 (2004) 135.
[182] D. Lewis, T. Pusztai, L. Gránásy, J.A. Warren, W.J. Boettinger, J. Metals, in press.
[183] J. Tiaden, B. Nestler, H.J. Diepers, I. Steinbach, Physica D 115 (1998) 73.
[184] J. Tiaden, U. Grafe, in: Proceedings of the International Conference on Solid-Solid Phase Transfor-mations, JIMIC-3, 1999.
[185] J.S. Lee, S.G. Kim, W.T. Kim, T. Suzuki, ISIJ Int. 39 (1999) 730.
[186] B. Nestler, A.A. Wheeler, L. Ratke, C. Stöcker, Physica D 141 (2000) 133.
[187] M. Plapp, A. Karma, Phys. Rev. E 66 (2002) 061608.
[188] R.S. Qin, E.R. Wallach, Acta Mater. 51 (2003) 6199.
[189] H. Kobayashi, M. Ode, S.G. Kim, W.T. Kim, T. Suzuki, Scripta Mater. 48 (2003) 689.
[190] Q. Chen, N. Ma, K. Wu, Y. Wang, Scripta Mater. 50 (2004) 471.
[191] P.-R. Cha, D.-H. Yeon, J.-K. Yoon, Acta Mater. 49 (2001) 3295.
[192] I. Steinbach, F. Pezzola, B. Nestler, M. Seesselberg, R. Prieler, G.J. Schmitz, J.L.L. Rezende, Physica D 94 (1996) 135.
[193] I. Steinbach, F. Pezolla, Physica D 134 (1999) 385.
[194] U. Grafe, B. Böttger, J. Tiaden, S.G. Fries, Scripta Mater. 42 (2000) 1179.
[195] B. Böttger, U. Grafe, D. Ma, S.G. Fries, Mater. Sci. Technol. 16 (2000) 1425.
[196] B. Böttger, U. Grafe, D. Ma, A. Schnell, in: Superalloys 2000, Met. Soc. AIME (2000) 313.
[197] B. Böttger, I. Steinbach, S.G. Fries, Q. Chen, B. Sundman, et al. in: J. Lecomte-Beckers (Ed.), Materials for Advanced Power Engineering 2002, part III, Forschungszentrum Jülich, Jülich, 2002, p. 1333.
[198] B. Böttger, Ph. Schaffnit, J. Eicken, unpublished work.
[199] W.C. Swope, H.C. Andersen, Phys. Rev. B 41 (1990) 7042.

[200] P.R. ten Wolde, D. Frenkel, Phys. Chem. Chem. Phys. 1 (1999) 2191.
[201] J. Farkas, Z. Phys. Chem. (Leipzig) 38 (1927) 236.
[202] R. Becker, W. Döring, Ann. Phys. 24 (1935) 719.
[203] D. Turnbull, J.C. Fisher, J. Chem. Phys. 17 (1949) 71.
[204] J.W. Christian, The Theory of Transformations in Metals and Alloys, Oxford Univ. Press, Oxford, 1975.
[205] J.M. Howe, Philos. Mag. A 74 (1996) 761.
[206] W.J. Huisman, J.F. Peters, M.J. Zwanenburg, S.A. de Vries, T.E. Derry, D. Abernathy, J.F. van der Veen, Nature 390 (1997) 379.
[207] B.B. Laird, A.D. Haymet, J. Chem. Rev. 92 (1992) 1819.
[208] J.D. Gunton, J. Stat. Phys. 95 (1999) 903.
[209] L. Gránásy, P.F. James, J. Chem. Phys. 113 (2000) 9810.
[210] Z. Kozisek, P. Demo, J. Chem. Phys. 102 (1995) 7695.
[211] G. Wilemski, B.E. Wyslouzil, J. Chem. Phys. 103 (1995) 1127.
[212] V.V. Slezov, J. Schmelzer, Y.Y. Tkatch, J. Chem. Phys. 105 (1996) 8340.
[213] Z. Kozisek, T. Koga, K. Sato, P. Demo, J. Chem. Phys. 114 (2001) 7622.
[214] V.V. Slezov, J. Schmelzer, Phys. Rev. E 65 (2002) 031506–031511.
[215] J.W.P. Schmelzer, A.R. Gokhman, V.M. Fokin, J. Coll. Interface Sci., in press.
[216] K. Binder, D. Stauffer, Adv. Phys. 25 (1976) 343.
[217] A.L. Greer, P.V. Evans, R.G. Hamerton, D.K. Shangguan, K.F. Kelton, J. Cryst. Growth 99 (1990) 38.
[218] K.F. Kelton, J. Non-Cryst. Solids 274 (2000) 147.
[219] L. Gránásy, Europhys. Lett. 24 (1993) 121.
[220] L. Gránásy, J. Chem. Phys. 104 (1996) 5188.
[221] L. Gránásy, F. Iglói, J. Chem. Phys. 107 (1997) 3634.
[222] T. Volkmann, W. Löser, D.M. Herlach, Metall. Mater. Trans. A 28 (1997) 453.
[223] S.A. Moir, D.M. Herlach, Acta Mater. 45 (1997) 2827.
[224] B. Kvamme, Int. J. Offshore Polar Eng. 11 (2002) 256.
[225] J.W.P. Schmelzer, J. Schmelzer, I.S. Gutzow, J. Chem. Phys. 112 (2000) 3820.
[226] B. Cantor, K.A.Q. O'Reilly, Curr. Opin. Solid State Mater. Sci. 2 (3) (1997) 318.
[227] A.L. Greer, A.M. Bunn, A. Tronche, P.V. Evans, D.J. Bristow, Acta Mater. 48 (2000) 2823.
[228] J.H. Perepezko, J.L. Sebright, G. Wilde, Adv. Eng. Mater. 4 (2002) 147.
[229] J.D. van der Waal, Verhand. Koninkl. Akad. Wetensch. Amsterdam 1 (1893) 1.
[230] J.W. Cahn, J.E. Hilliard, J. Chem. Phys. 31 (1959) 688.
[231] C.K. Bagdassarian, D.W. Oxtoby, J. Chem. Phys. 100 (1994) 2139.
[232] L. Gránásy, D.W. Oxtoby, J. Chem. Phys. 112 (2000) 2399.
[233] R. Wild, P. Harrowell, Phys. Rev. E 56 (1997) 3265.
[234] L. Gránásy, T. Pusztai, P.F. James, J. Chem. Phys. 117 (2002) 6157.
[235] L. Gránásy, T. Börzsönyi, T. Pusztai, Phys. Rev. Lett. 88 (2002) 206105–206111.
[236] R. Kobayashi, J.A. Warren, W.C. Carter, Physica D 119 (1998) 415.
[237] R. Kobayashi, J.A. Warren, W.C. Carter, Physica D 140 (2000) 141.
[238] A. Roy, J.M. Rickman, J.D. Gunton, K.R. Elder, Phys. Rev. 56 (1998) 2610.
[239] L. Gránásy, T. Pusztai, G. Tóth, Z. Jurek, M. Conti, B. Kvamme, J. Chem. Phys. 119 (2003) 10376.
[240] L. Gránásy, T. Pusztai, J. Chem. Phys. 117 (2002) 10121.
[241] P.J. Simmons, C. Shen, Y. Wang, Scripta Mater. 43 (2000) 935.
[242] D. Turnbull, J. Chem. Phys. 20 (1952) 411.
[243] L. Gránásy, T. Pusztai, J.A. Warren, T. Börzsönyi, J.F. Douglas, V. Ferreiro, Nature Mater. 2 (2003) 92.
[244] M. Castro, Phys. Rev. B 67 (2003) 035412.
[245] L. Gránásy, T. Pusztai, J.A. Warren, in press.
[246] C.S. Smith, Metall. Rev. 9 (1964) 1.
[247] U. Hecht, V.T. Witusiewicz, S. Rex, in: B.K. Dhindaw (Ed.), International Conference on Solidification Science and Processing, Science Publisher Inc., Bangalore, 2001, p. 61.
[248] J. Alkemper, S. Sous, C. Stöcker, L. Ratke, J. Cryst. Growth 191 (1998) 252.
[249] P.A. Curreri, W.F. Kaukler, Metall. Mater. Trans. 27A (1996) 801.
[250] R.H. Mathiesen, L. Arnberg, F. Mo, T. Weitkamp, A. Snigirev, Phys. Rev. Lett. 83 (1999) 5062.
[251] G. Zimmermann, A. Schievenbusch, A. Drevermann, in: Proceedings of 2nd European Symposium on the Utilisation of the ISS, ESTEC, Noordwijk, The Netherlands (ESA SP-433), 1999, p. 377.

[252] C. Salvi, B. Drevet, J.P. Garandet, G. Quillet, P. Lehmann, in: Proceedings of the First International Symposium on Microgravity Research & Applications in Physical Sciences & Biotechnology, Sorrento, Italy (ESA SP-454, January 2001), 10–15 September 2000, p. 715.
[253] J.P. Garandet, C. Salvi, Int. J. Heat Mass Transfer 45 (2002) 1045.
[254] G. Amberg, Phys. Rev. Lett. 91 (2004) 265505.
[255] K.R. Elder, M. Katakowski, M. Haataja, M. Grant, Phys. Rev. Lett. 88 (2002) 245701.
[256] K. R. Elder, M. Grant, Phys. Rev. E, in press (preprint cond-mat/0107381).
[257] K.R. Elder, personal communication, 2004.